

DISSERTATION

submitted

to the

Combined Faculty for the Natural Sciences and Mathematics

of

Heidelberg University, Germany

for the degree of

Doctor of Natural Sciences

Put forward by

M.S. Mathematics **Noman Shakir**

Born in Attock, Pakistan

Oral examination:

Multilevel Schwarz Methods for Incompressible Flow Problems

Advisor: Prof. Dr. Guido Kanschat

Co-Advisor: Prof. Dr. Oleg Iliev

To my parents

M. Taj Shakir and Sadri Baigum

Acknowledgment

I remain highly indebted to Prof. Dr. Guido Kanschat for his support and feedback at every stage of this study. From the initial conceptualization to final revision, his help remained invaluable. I could have hardly imagined a better supervisor. The kind support and help of Prof. Dr. Oleg Oliev, the co-advisor of this work, is gratefully acknowledged.

Special thanks are due to my group members, especially Dr. Arbaz Khan, Dr. Danial Arndt and Julius, for their useful inputs and suggestions. Dr. Joscha Gedicke and Pablo deserve a special mention for fruitful discussions on implementation aspects.

The research infrastructure and resources provided by the Interdisciplinary Scientific Computing Center (IWR), Heidelberg University were second to none. Further, I remain thankful to Dr. Michael Winkler for his counseling, especially concerning financial matters. Importantly, my doctoral work was made possible by financial grants from Erasmus Mundus Mobility with Asia (EMMA), Heidelberg Graduate School (HGS MathComp) and the Chair of Mathematical Methods of Simulation. I am also thankful to the Faculty of Mathematics and Computer Science for administrating the formalities of my doctorate.

Finally, I would like to thank my wife Sadia, my daughter Fatima, and my friends in Heidelberg. Their influence is not visible in this work, but, without their social support, tolerance, and empathy, it would have been very difficult - if not impossible - to write this thesis.

Contents

Acknowledgement	i
Abstract	v
1 Introduction	1
1.1 Outline	4
2 Mathematical Framework	7
2.1 Function Spaces	7
2.1.1 Sobolev Spaces	7
2.1.2 Finite Element Spaces	8
2.1.3 Raviart-Thomas spaces	9
2.2 Multilevel Meshes	10
2.3 DG Notations	10
3 The Oseen Equations	12
3.1 Introduction	12
3.2 Model Problem	13
3.3 Discontinuous Galerkin discretization	13
3.4 Existence and Uniqueness of Solution	15

3.5	The singularly perturbed problem	17
3.6	Overlapping Schwarz Smoothers	18
3.6.1	Projection Operators	19
3.6.2	Multiplicative Schwarz	21
3.6.3	Convergence Analysis	22
3.7	Multigrid preconditioner	25
3.7.1	Projection Operators	25
3.7.2	V-cycle Algorithm	26
3.7.3	Recurrence Relation	28
3.7.4	Convergence Analysis	29
3.7.5	Downwind Ordering	30
3.8	Numerical Results	30
3.8.1	Poisseeuille Flow	31
3.8.2	Kovaszny Flow	32
3.8.3	Multigrid Performance	34
3.9	Summary	40
4	The Navier-Stokes Equations	42
4.1	Introduction	42
4.2	Model Problem	43
4.3	Discontinuous Galerkin discretization	43
4.4	Existence and Uniqueness of Solution	44
4.5	Overlapping Schwarz Smoothers	45
4.6	Multigrid preconditioner	46
4.7	Numerical Results	48
4.7.1	Poisseeuille Flow	48

4.7.2	Kovaszny Flow	49
4.7.3	Multigrid Performance	50
4.8	Summary	62
5	The Brinkman Equations	64
5.1	Introduction	64
5.2	Linear Brinkman	65
5.2.1	Model Problem	65
5.2.2	Discontinuous Galerkin discretization	66
5.2.3	Existence and Uniqueness of Solution	67
5.2.4	Overlapping Schwarz Smoothers	69
5.2.5	Multigrid preconditioner	69
5.2.6	Numerical Results	71
5.3	Nonlinear Brinkman	80
5.3.1	Discontinuous Galerkin discretization	81
5.3.2	Multigrid preconditioner	81
5.3.3	Numerical Results	83
5.4	Summary	88
6	Summary	89

Abstract

In this thesis, we address coupled incompressible flow problems with respect to their efficient numerical solutions. These problems are modeled by the Oseen equations, the Navier-Stokes equations and the Brinkman equations. For numerical approximations of these equations, we discretize these systems by H^{div} -conforming discontinuous Galerkin method which globally satisfy the divergence free velocity constraint on discrete level. The algebraic systems arising from discretizations are large in size and have poor spectral properties which makes it challenging to solve these linear systems efficiently.

For efficient solution of these algebraic system, we develop our solvers based on classical iterative solvers preconditioned with multigrid preconditioners employing overlapping Schwarz smoothers of multiplicative type. Multigrid methods are well known for their robustness in context of self-adjoint problems. We present an overview of the convergence analysis of multigrid method for symmetric problems. However, we extend this method to non self-adjoint problems, like the Oseen equations, by incorporating the downwind ordering schemes of Bey and Hackbusch and we show the robustness of this method by empirical results.

Furthermore, we extend this approach to non-linear problems, like the Navier-Stokes and the non-linear Brinkman equations, by using a Picard iteration scheme for linearization. We investigate extensively by performing numerical experiment for various examples of incompressible flow problems and show by empirical results that the multigrid method is efficient and robust with

respect to the mesh size, the Reynolds number and the polynomial degree. We also observe from our numerical results that in case of highly heterogeneous media, multigrid method is robust with respect to a high contrast in permeability.

Zusammenfassung

Diese Arbeit beschäftigt sich mit Methoden zum effektiven Lösen von Gleichungen, die aus gekoppelten inkompressiblen Strömungsproblemen resultieren. Dabei handelt es sich genauer um die Oseen-, Navier-Stokes- und Brinkmangleichungen. Zur Approximation der Lösung dieser Gleichungen verwenden wir H^{div} -konforme unstetige finite Elemente, welche die Inkompressibilitätsnebenbedingung global erfüllen. Die großen Dimensionen und die schlechte Kondition der korrespondierenden linearen Gleichungssysteme machen das effiziente Lösen zu einer herausfordernden Aufgabe.

Zum effektiven Lösen der Gleichungssysteme entwickeln wir unsere Löser basierend auf klassischen iterativen Lösern mit Mehrgittervorkonditionieren, die multiplikative Schwarz-Glätter benutzen. Mehrgittermethoden sind wohlbekannt für ihre Robustheit im Kontext selbstadjungierter Probleme. Wir präsentieren einen Überblick über die Konvergenzanalyse für symmetrische Probleme. Für nicht selbstadjungierte Probleme, wie den Oseengleichungen, benutzen wir die Downwind-Sortierung nach Bey und Hackbusch und zeigen die Robustheit der resultierenden Methode empirisch.

Darüber hinaus erweitern wir diesen Ansatz auf nichtlineare Probleme, wie die Navier-Stokes- oder die nichtlinearen Brinkmangleichungen, wobei eine Picarditeration zur Linearisierung benutzt wird. Wir untersuchen diesen Algorithmus eingehend mit numerischen Experimenten für verschiedene Beispiele inkompressibler Strömungsprobleme und zeigen mit empirischen Resultaten, dass das Mehrgitterverfahren effizient und robust im Bezug auf Gitterweite,

Reynoldszahl und Polynomgrad ist. Wir beobachten in unseren numerischen Resultaten, dass das Mehrgitterverfahren auch für stark heterogene Materialien robust im Bezug auf den Quotienten der Permeabilitätskoeffizienten ist.

List of Figures

2.1	Degrees of freedom of Raviart-Thomas elements for order 0,1 and 2 are 4, 12 and 24 respectively	9
2.2	Multi-level meshes from left to right for levels $\ell = 0, 1, 2$	10
2.3	Two adjacent mesh cells	11
3.1	Subdomains consisting of vertex patches	19
3.2	Velocity stream lines for Kovasznay flow	33
4.1	Velocity magnitude for Kovasznay flow	50
4.2	Velocity magnitude for Cavity driven flow	59
4.3	Geometry of Problem	60
4.4	Velocity magnitude for flow behind an obstacle, top to bottom $Re = 1, 10, 50, 100, 200$	61
4.5	Streamlines for velocity profiles for Obstacle Problem $Re = 10$ (top) and $Re = 100$ (bottom)	62
5.1	Inverse Permiability coefficient (κ) distribution	71
5.2	Upscaling and downscaling	73
5.3	Darcy: Solution for Sparse periodic geometry	75
5.4	Darcy: Solution for Dense periodic geometry	76

5.5	Brinkman: Solution for Sparse periodic geometry	78
5.6	Brinkman: Solution for Dense periodic geometry	79
5.7	Nonlinear Brinkman: Solution in Sparse periodic geometry . .	85
5.8	Nonlinear Brinkman: Solution in Dense periodic geometry . .	87

List of Tables

3.1	Convergence rates of errors for Poiseuille flow	32
3.2	Convergence rates of errors for Kovasznay flow	34
3.3	GMRES iterations for variation of parameter ν with and without sorting	35
3.4	Iteration count for different Reynolds numbers using $RT_1 \times Q_1$ for Poiseuille flow function with $m(\ell) = 1$	36
3.5	Iteration count for different Reynolds numbers using $RT_1 \times Q_1$ for Poiseuille flow function with $m(\ell) = 2$	36
3.6	Iteration count for different Reynolds numbers using $RT_1 \times Q_1$ for Kovasznay flow function with $m(\ell) = 1$	37
3.7	Iteration count for different Reynolds numbers using $RT_1 \times Q_1$ for Kovasznay flow function with $m(\ell) = 2$	38
3.8	Number of iterations for different relaxation parameters	38
3.9	GMRES iterations for FE pair $RT_k \times Q_k$	39
3.10	Comparison of multigrid preconditioners with block preconditioners	40
4.1	Convergence rates for L^2 and H^1 errors of velocity and pressure	48

4.2	Convergence rates for L^2 and H^1 errors of velocity and pressure	49
4.3	Comparison of vertex patches sorting with no sorting	51
4.4	Sorting in one direction, $m(\ell) = 1$	52
4.5	Full sweep, $m(\ell) = 1$	53
4.6	Full sweep, $m(\ell) = 2$	54
4.7	Sweep in 2 directions, $m(\ell) = 1$	55
4.8	Sweep in 2 directions, $m(\ell) = 2$	56
4.9	Cavity driven flow	58
4.10	Flow behind an obstacle	60
5.1	Darcy: GMRES iteration count for different inverse permeability coefficient κ for Sparse periodic geometry	73
5.2	Brinkman: GMRES iteration count for different inverse permeability coefficient κ for Dense periodic geometry	74
5.3	Iteration count of Picard iteration and GMRES for Sparse periodic geometry	84
5.4	Iteration count of Picard iteration and GMRES for Dense periodic geometry	86

Chapter 1

Introduction

In this thesis, we develop a methodology for the efficient numerical solutions of large algebraic systems arising from discretizations of the Oseen, the Navier-Stokes and the Brinkman equations. We use multigrid preconditioners with overlapping Schwarz smoothers. Robustness with respect to the mesh parameters of the multigrid method is shown by empirical results.

Fluid flow is an essential part of many applications, e.g. aerodynamics, natural convection in the earth's mantle or flows in industrial foams. It is often complicated and expensive to imitate these flows in experiments, if not impossible. Therefore, the numerical simulations are an important tool to complement the experiments or to replace them.

With modern computers and their capabilities, large scale simulations in Computational Fluid Dynamics (CFD) have garnered considerable attention in recent years. There are two major aspects in CFD. First, it is based on

proper mathematical modeling of physical phenomena. Second, it is based on efficient implementation of the derived algorithms. The focus in this manuscript is the latter aspect of CFD.

The Navier-Stokes equations are used as a mathematical model for incompressible fluid flow and have many applications in real-world problems. Therefore, efficient simulation methods for the Navier-Stokes equations are of great importance.

We develop a methodology for solving the Navier-Stokes equations efficiently in the first part of this thesis. We start with a linearized version of the Navier-Stokes equations, namely the Oseen equations. The finite element discretization of such equations leads to large algebraic systems with poor spectral properties [16, 64]. Hence, it becomes challenging to solve these large algebraic systems efficiently. In order to solve such algebraic systems, preconditioning techniques are required [30, 31, 35, 49, 72]. In our methodology, we use the multigrid preconditioners with overlapping Schwarz smoothers [8, 10]. Such preconditioners have proven to be efficient, theoretically and numerically, for symmetric problems e.g. [8, 10, 33, 42, 43, 52, 59, 67, 68]. However, for non-symmetric problems, like the Oseen equations, there are no existing results for efficiency of this multigrid method, either theoretical or numerical.

We extend this method to non-symmetric problems by incorporating the downwind ordering schemes of Bey and Hackbush [12, 37]. These re-ordering techniques have proven to be efficient for obtaining robust multigrid methods

for advection dominated cases in advection-diffusion problems, for instance in [50]. Nevertheless, for the Oseen equations, we extend the idea of applying downwind ordering to vertex patches, namely subdomains in context of Schwarz smoothers, for smoothing operations in multigrid method. Our numerical results show that the multigrid preconditioner is efficient as compared to the block preconditioners [35, 55, 62]. Moreover, it is robust with respect to the mesh size, the Reynolds number and the polynomial degree.

For the Navier-Stokes equations, we encounter additional problems due to the nonlinear convection term. For linearization, we use the classical Picard iteration, following the approach in [22], where multigrid preconditioner is used in each iteration for solving the linear system. In this case, we show efficiency of the multigrid method by the numerical results for different fluid flow problems. Whereas, robustness of the multigrid method with respect to the mesh size for high Reynolds numbers is still an open question.

In the second part of this thesis, we extend our numerical experiments to show the efficiency of the multigrid methods for fluid flow problems in heterogeneous porous media. There are many real-world application in which mathematical models and simulations of flow through porous media are of great importance. Examples include ecology, underground water flow, industrial filters and oil exploration etc. Hence, many researchers search for better mathematical models and efficient algorithms for these flow problems.

Mathematically, fluid flow through porous media is described by the Darcy's

law on the macro level neglecting viscous effects. In 1947, Brinkman [17] proposed a model for fluid flow through porous media which also takes into account viscous effects. The Brinkman model is widely used for fluid flow problems in highly porous media, whereas for low porosity and low Reynolds numbers the Darcy model is still considered to be appropriate.

We consider two cases: the linear Brinkman equations (neglecting the convection term) and the nonlinear Brinkman equations (including the convection term). We use the same multigrid setting for solving algebraic systems, arising from the discretizations of the Brinkman equations in both cases. Multigrid methods have recently proven to be efficient by Kanschat and Mao [51] for the linear Brinkman equations. We extend this approach of multigrid methods to the nonlinear Brinkman equations using the classical Picard iteration. We show by empirical results that the multigrid method is robust with respect to the mesh size and variations in permeability.

1.1 Outline

In Chapter 2, we present basic definitions of function spaces and finite element spaces. We also set some basic notation for discontinuous Galerkin discretization and multi-level meshes, those are used throughout this manuscript.

In Chapter 3, we present the multigrid method with overlapping Schwarz smoothers for the Oseen equations. The system is discretized by H^{div} -conforming discontinuous elements and the resulting linear problem is solved

by using multigrid preconditioner with overlapping Schwarz smoothers. We provide an overview of the convergence analysis for multigrid preconditioner for symmetric problems given in [52]. We perform extensive numerical experiments using the multigrid method for the Oseen equations. We observe that our solver is robust with respect to the mesh size, the Reynolds number and the polynomial degree. This implies that the numerical results for non-symmetric problems are in agreement with the theory for symmetric problems.

In Chapter 4, we extend our numerical experiments to the nonlinear problems, namely the Navier-Stokes equations. We use the same discretization as in case of the Oseen equations and the resulting linear problem is solved by using multigrid preconditioner with overlapping Schwarz smoothers of multiplicative type. We use the classical Picard iteration for linearizing and GMRES [66] in combination with multigrid preconditioner as inner solver for the linear system. Finally, we present numerical results for a variety of flow problems. These results show that for the Navier-Stokes equations, robustness of the multigrid preconditioner depends on mesh parameters and the Reynolds number. Nevertheless, it is still efficient.

In Chapter 5, we present the multigrid preconditioner for the finite element approximation of flow problems in highly heterogeneous porous media governed by the Brinkman equations. In Section 5.2, we describe the multigrid method for the linear Brinkman equations (neglecting the convection term) and present the corresponding numerical results. In Section 5.3, we use the

same multigrid method for the nonlinear Brinkman equations (including the convection term) and we present the numerical results. In both cases, we observe from the computational results that the multigrid method is robust with respect to the mesh size and variations in permeability for highly heterogeneous porous media.

The thesis is concluded by summarizing its findings and points towards the importance of extending its contribution.

Chapter 2

Mathematical Framework

In this chapter, we provide an overview of some basic definitions of function spaces, widely used in this script later on. We introduce some notations especially for discontinuous Galerkin and multilevel meshes. We will follow these definitions and notations in later chapters.

2.1 Function Spaces

In this section we provide an overview of some existing theory about the function spaces.

2.1.1 Sobolev Spaces

The natural spaces for variational problems are Sobolev spaces [1]. We consider a Lipschitz domain $\Omega \subset \mathbb{R}^d$ where d is 2 or 3. We start with L^2 -spaces in this domain. The $L^2(\Omega)$ is a space of square integrable functions on domain

Ω with the following norm.

$$\|u\|_0 = \int_{\Omega} |u|^2 dx \quad \text{for } u \in L^2(\Omega)$$

The space $H^1(\Omega)$ is the space of all functions which have weak gradient. So we have the following norm for this space

$$\|u\|_1 = \int_{\Omega} |u|^2 dx + \int_{\Omega} |\nabla u|^2 dx \quad \text{for } u \in H^1(\Omega)$$

Then we have $H_0^1(\Omega)$ which is the space of the functions $u \in H^1(\Omega)$ such that $u|_{\partial\Omega} = 0$. Here $u|_{\partial\Omega}$ in sense of traces and $u|_{\partial\Omega}$ for $u \in H^1(\Omega) \cap C^0(\bar{\Omega})$ coincide.

2.1.2 Finite Element Spaces

For the discretization of our model problems on mesh \mathcal{T}_ℓ , we choose discrete subspace $S_\ell = V_\ell \times Q_\ell$ where $Q_\ell \subset Q$. Following [22] and [52] for the divergence free velocity we consider the discrete subspace V_ℓ of the space $H_0^{div}(\Omega)$, where

$$\begin{aligned} H^{div}(\Omega) &= \{v \in L^2(\Omega; \mathbb{R}^d) \mid \nabla \cdot v \in L^2(\Omega)\}, \\ H_0^{div}(\Omega) &= \{v \in H^{div}(\Omega) \mid v \cdot \mathbf{n} = 0 \text{ on } \partial\Omega\}. \end{aligned}$$

Here, we observe that any pair of the velocity spaces V_ℓ and pressure Q_ℓ is admissible, if the key relation

$$\nabla \cdot V_\ell = Q_\ell \tag{2.1}$$

holds.

2.1.3 Raviart-Thomas spaces

We choose the well known Raviart-Thomas space [65]. The details of constructing the Raviart-Thomas space follow as in [52].

We define on the reference cell $\hat{T} = [0, 1]^d$ two polynomial spaces \hat{Q}_k and \hat{V}_k such that first is the space of polynomials in d variables each with maximum degree k and second is the vector valued Raviart-Thomas space $\hat{V}_k = \hat{Q}_k^d + x\hat{Q}_k$. Now, for each cell $T \in \mathcal{T}_\ell$, we have a linear mapping Ψ_T such that $T = \Psi_T(\hat{T})$ through which we get polynomial spaces V_T and Q_T on the mesh cell T . As the polynomial degree k is chosen uniformly for the whole mesh so we omit index k from now on. By this construction we get the following pair of finite element spaces.

$$V_\ell = \{v \in H_0^{div}(\Omega) \mid \forall T \in \mathcal{T}_\ell : v|_T \in V_T\},$$

$$Q_\ell = \{q \in L_0^2(\Omega) \mid \forall T \in \mathcal{T}_\ell : q|_T \in Q_T\}.$$

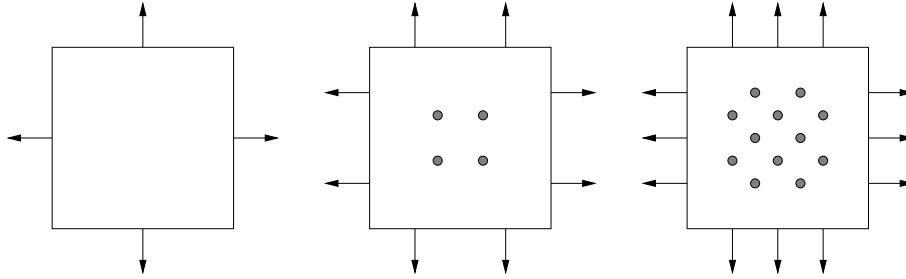


Figure 2.1: Degrees of freedom of Raviart-Thomas elements for order 0,1 and 2 are 4, 12 and 24 respectively

2.2 Multilevel Meshes

For the finite element discretization, we make a hierarchy of meshes $\{\mathcal{T}_\ell\}_{\ell=0,\dots,L}$ on the domain Ω where ℓ indicates the mesh level in multilevel method such that by going from level ℓ to level $\ell + 1$ mesh is refined once in a way such that each cell is divided into 2^d cells(children) so that we obtain the nested meshes. The mesh size h_ℓ is defined as the maximum of the diameter of the cells at level ℓ .

Through this process of refinement we construct the conforming meshes, so

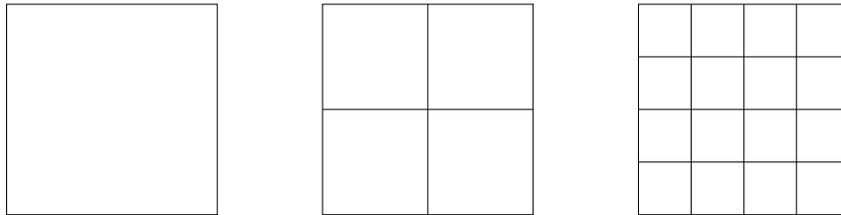


Figure 2.2: Multi-level meshes from left to right for levels $\ell = 0, 1, 2$

every face of a cell is either at boundary or a whole face of another cell. The notation for the set of all faces will be \mathcal{F}_ℓ and $\mathcal{F}_\ell = \mathcal{F}_\ell^i \cup \mathcal{F}_\ell^\partial$, sum of interior and boundary faces.

2.3 DG Notations

We define the averaging operator $\{\!\!\{ \cdot \}\!\!\}$ and the jump $\llbracket \cdot \rrbracket$ over the face F between two adjacent cells T_1 and T_2 (Fig. 2.3) as follow:

$$\{\!\!\{ u \}\!\!\} = \frac{u_1 + u_2}{2} \quad \llbracket u \rrbracket = u_1 - u_2$$

where u_1 and u_2 are the traces of u from T_1 and T_2 on the joint face F .

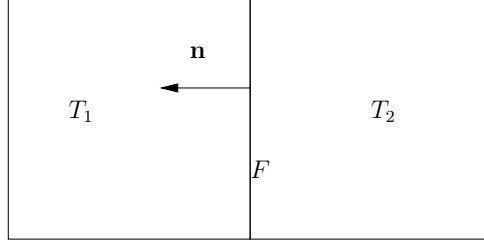


Figure 2.3: Two adjacent mesh cells

We introduce a short hand notation for the integral forms on \mathcal{T}_ℓ and on \mathcal{F}_ℓ by

$$(\phi, \psi)_{\mathcal{T}_\ell} = \sum_{T \in \mathcal{T}_\ell} \int_T \phi \odot \psi dx, \quad \langle \phi, \psi \rangle_{\mathcal{F}_\ell} = \sum_{F \in \mathcal{F}_\ell} \int_F \phi \odot \psi ds,$$

$$\|\phi\|_{\mathcal{T}_\ell} = \left(\sum_{T \in \mathcal{T}_\ell} \int_T |\phi|^2 dx \right)^{\frac{1}{2}}, \quad \|\phi\|_{\mathcal{F}_\ell} = \left(\sum_{F \in \mathcal{F}_\ell} \int_F |\phi|^2 dx \right)^{\frac{1}{2}}.$$

The point-wise multiplication operator $\phi \odot \psi$ refers to the product $\phi\psi$, the scalar product $\phi\dot{\psi}$ and the double contraction $\phi : \psi$ for scalar, vector and tensor arguments respectively. The modulus $|\phi| = \sqrt{\phi \odot \psi}$ is defined accordingly.

Chapter 3

The Oseen Equations

3.1 Introduction

In this chapter, the multigrid method with overlapping Schwarz smoothers for the Oseen equations is presented. The system is discretized by H^{div} -conforming discontinuous Galerkin method and the resulting linear problem is solved by using a multigrid preconditioner employing overlapping multiplicative Schwarz smoothers. An overview of the convergence analysis of multigrid preconditioner for symmetric problems is presented which shows the robustness of the multigrid method. We extend this method to non-symmetric problems by apply the downwind ordering schemes of Bey and Hackbusch. We show the robustness of multigrid method by performing extensive numerical experiments for the case of non-symmetric problems, like the Oseen equations. We observe the efficiency of multigrid preconditioners as compare to block preconditioners [35, 55]. Furthermore, we see that, with multigrid preconditioners, the work required by linear solver - in case of the

Oseen equations - is nearly same as for Laplace problem. Moreover, our numerical results show that the multigrid method is robust with respect to the mesh size, the Reynolds number and the polynomial degree.

3.2 Model Problem

The Oseen equations are

$$\begin{aligned} -\nu\Delta u + (\beta \cdot \nabla) u + \gamma u + \nabla p &= \mathbf{f} && \text{in } \Omega, \\ \nabla \cdot u &= 0 && \text{in } \Omega, \\ u &= \mathbf{g} && \text{on } \partial\Omega, \end{aligned} \quad (3.1)$$

where u , p and $\mathbf{f} \in L^2(\Omega)^d$ are velocity, pressure and prescribed external body force, respectively. Here ν is the kinematic viscosity, β is a convective velocity field and γ is a given scalar function and we assume that

$$\gamma(\mathbf{x}) - \frac{1}{2}\nabla \cdot \beta(\mathbf{x}) = \gamma_0(\mathbf{x}) \geq 0 \quad \mathbf{x} \in \Omega. \quad (3.2)$$

As in [23] and the references therein, the condition (3.2) guarantees the existence and uniqueness of the solution $(u, p) \in (V = H_0^1(\Omega)^d, Q = L_0^2(\Omega))$, where $\Omega \subset \mathbb{R}^d$ is a bounded and convex domain with no-slip boundary conditions.

3.3 Discontinuous Galerkin discretization

We use a divergence conforming discontinuous Galerkin discretization for (3.1), by following the examples in [22, 48, 52, 53, 54]. For this type of

discretization weakly divergence free functions are point-wise divergence free. Such discretizations are available in literature, for instance, in Scott and Vogelius [70, 75], Neilan *et al.* [32, 36] and Zhang [81, 82]. The Laplacian term is discretized by means of the interior penalty method [9, 63]. Using the notations defined in Section 2.3 for jumps and averages, the interior penalty bilinear form for the Laplacian term and the upwinding bilinear form for the convection term can be written as

$$\begin{aligned} a_\ell(u, v) &= \nu (\nabla u, \nabla v)_{\mathcal{T}_\ell} + 4 \langle \sigma_\ell \{ \{ u \otimes \mathbf{n} \} \}, \{ \{ v \otimes \mathbf{n} \} \} \rangle_{\mathcal{F}_\ell^i} \\ &\quad - 2 \langle \{ \{ \nabla u \} \}, \{ \{ \mathbf{n} \otimes v \} \} \rangle_{\mathcal{F}_\ell^i} - 2 \langle \{ \{ \nabla v \} \}, \{ \{ \mathbf{n} \otimes u \} \} \rangle_{\mathcal{F}_\ell^i} \\ &\quad + 2 \langle \sigma_\ell u, v \rangle_{\mathcal{F}_\ell^\partial} - \langle \partial_n u, v \rangle_{\mathcal{F}_\ell^\partial} - \langle \partial_n v, u \rangle_{\mathcal{F}_\ell^\partial}, \end{aligned}$$

$$\begin{aligned} b_\ell(\beta; u, v) &= (\gamma u, v)_{\mathcal{T}_\ell} - (u, \nabla \cdot v \otimes \beta)_{\mathcal{T}_\ell} \\ &\quad + 2 \langle | \beta \cdot \mathbf{n} | u^\uparrow, [v] \rangle_{\mathcal{F}_\ell^i} + 2 \langle | \beta \cdot \mathbf{n} | u, v \rangle_{\mathcal{F}_\ell^\partial}. \end{aligned}$$

The operator \otimes denotes the Kronecker product of the two vectors. We note that the term $4 \{ \{ u \otimes \mathbf{n} \} \} : \{ \{ v \otimes \mathbf{n} \} \}$ actually denotes the jumps of u and v . To ensure the coercivity of form $a_\ell(\cdot, \cdot)$, the interior penalty parameter σ_ℓ has to be chosen sufficiently large. We can estimate its lower limit by

$$\sigma_\ell > \frac{k(k+1)}{2h_\ell}.$$

Where k is the degree of the polynomial and h_ℓ is the mesh size at level ℓ . We usually choose twice the value in our numerical test.

The discrete weak formulation of (3.1) reads now: find $(u_\ell, p_\ell) \in V_\ell \times Q_\ell$ such that for all test functions $v_\ell \in V_\ell$ and $q_\ell \in Q_\ell$ there holds

$$\mathcal{A}_\ell \left(\begin{pmatrix} u_\ell \\ p_\ell \end{pmatrix}, \begin{pmatrix} v_\ell \\ q_\ell \end{pmatrix} \right) = \mathcal{F}(v_\ell, q_\ell) \quad \forall v_\ell \in V_\ell, q_\ell \in Q_\ell, \quad (3.3)$$

where

$$\mathcal{A}_\ell \left(\begin{pmatrix} u_\ell \\ p_\ell \end{pmatrix}, \begin{pmatrix} v_\ell \\ q_\ell \end{pmatrix} \right) \equiv a_\ell(u_\ell, v_\ell) + b_\ell(\beta; u_\ell, v_\ell) + (p_\ell, \nabla \cdot v_\ell) - (q_\ell, \nabla \cdot u_\ell),$$

$$\mathcal{F}(v_\ell, q_\ell) \equiv (f, v_\ell).$$

3.4 Existence and Uniqueness of Solution

In this section, we present an overview of the theory for the existence and uniqueness of discrete solution as discussed in [22, 24, 41, 53]. We use the finite element spaces RT_k/Q_k , as described in Section 2.1.2. Thus for pair of Raviart-Thomas spaces, we have

$$\nabla \cdot RT_k = Q_k.$$

The resulting space V_ℓ is equipped with the norm

$$\|u\|_\sigma^2 = \sum_{T \in \mathcal{T}_\ell} \|\nabla u\|_{L^2(T)}^2 + \sum_{F \in \mathcal{F}_\ell} \int_F \sigma_L |\{u \otimes \mathbf{n}\}|^2 ds.$$

For the existence and uniqueness of discrete solution, we need continuity and coercivity of the form $\mathcal{A}_\ell(\cdot, \cdot)$ for which we have following estimates for the diffusion term, the convection term and incompressibility constraint. For proofs of the following proposition we refer to [21, 22].

Proposition 3.4.1. *If the interior penalty (IP) parameter is chosen sufficiently large, then there exist constants $c_a >$ and $\alpha > 0$, independent of the*

viscosity and the mesh size, such that

$$\begin{aligned} a_\ell(u, v) &\leq \nu c_a \|u\|_\sigma \|v\|_\sigma & u, v \in V_\ell, \\ a_\ell(u, u) &\geq \nu \alpha \|u\|_\sigma^2 & u \in V_\ell. \end{aligned}$$

Proposition 3.4.2. *For any divergence free velocity field β and any $u \in V_\ell$ we have*

$$b_\ell(\beta; u, u) \geq 0.$$

Furthermore, if we also have that $\beta_1, \beta_2, v \in V_\ell$, it holds

$$|b_\ell(\beta_1; u, v) - b_\ell(\beta_2; u, v)| \leq c_0 \|\beta_1 - \beta_2\|_\sigma \|u\|_\sigma \|v\|_\sigma.$$

Proposition 3.4.3. *For any pressure function $q \in Q_\ell$, there exists a velocity function $v \in V_\ell$, satisfying*

$$\inf_{q \in Q_\ell} \sup_{v \in V_\ell} \frac{(q, \nabla \cdot v)}{\|v\|_\sigma \|q\|_{L^2(\Omega)}} \geq \gamma_\ell > 0,$$

where $\gamma_\ell = c \sqrt{\frac{h_L}{h_\ell}} = c \sqrt{2^{L-\ell}}$ and c is a constant independent of the multigrid level ℓ .

Proof. For the proof we refer to [69]. □

By using these propositions and the analysis given in ([22], Theorem 3.1) we obtain the result that there exist a unique solution for discontinuous Galerkin discretization of (3.3).

3.5 The singularly perturbed problem

For the multigrid analysis, we introduce the singularly perturbed problem related to (3.3). This makes it easy to carry the analysis in only velocity space V_ℓ . Afterwards, we show the equivalence of both solutions of original problem and singularly perturbed problem. The singularly perturbed problem, as in [34], has the following form

$$a_\ell(u_\ell, v_\ell) + b_\ell(\beta; u_\ell, v_\ell) + (p_\ell, \nabla \cdot v_\ell) = (f, v_\ell), \quad (3.4)$$

$$-\epsilon(p_\ell, q_\ell) + (q_\ell, \nabla \cdot u_\ell) = 0. \quad (3.5)$$

From (3.5), we have the relation $p_\ell = \epsilon^{-1} \nabla \cdot u_\ell$. By substituting this value of p_ℓ in (3.4), we have the following simpler penalty bilinear form

$$A_{\ell, \epsilon}(u_\ell, v_\ell) \equiv a_\ell(u_\ell, v_\ell) + b_\ell(\beta; u_\ell, v_\ell) + \epsilon^{-1}(\nabla \cdot u_\ell, \nabla \cdot v_\ell) = (f, v_\ell), \quad (3.6)$$

and the singularly perturbed problem: find $u_\ell \in V_\ell$ such that for all $v_\ell \in V_\ell$ there holds

$$A_{\ell, \epsilon}(u_\ell, v_\ell) = (f, v_\ell). \quad (3.7)$$

Then for the equivalence of the solutions, we have the following lemma as presented in [52] for the Stokes problem.

Lemma 3.5.1. *Let (u_m, p_m) be the solution to (3.4)-(3.5) and u_e be the solution to (3.7). Then, if (2.1) holds, the following equations hold true:*

$$u_m = u_e, \quad \text{and} \quad \epsilon p_m = \nabla \cdot u_m = \nabla \cdot u_e.$$

Proof. Proof of this lemma is simple by following the approach from [52], in spite of the fact that here we additionally have convection term. Nevertheless, it goes off in case of testing with $v_\ell = 0$ so rest of the proof is same. \square

Notations: For the following sections, we would like to introduce the separate notations for the mixed problem and singularly perturbed problem. We drop the subscript ϵ wherever possible. Furthermore, curly letters refer to the mixed form, while capitals refer to operators on the velocity space only. Thus:

- $a_\ell(u, v)$ is the vector valued interior penalty form.
- $A_\ell(u, v)$ is the form of the singularly perturbed problem (3.7).
- $\mathcal{A}_\ell\left(\begin{smallmatrix} u \\ p \end{smallmatrix}, \begin{smallmatrix} v \\ q \end{smallmatrix}\right)$ is the mixed bilinear form (3.3).

Additionally, we associate operators with bilinear forms using the same symbol:

$$\begin{aligned} A_\ell : V_\ell &\rightarrow V_\ell & (A_\ell u, v) &= A_\ell(u, v) & \forall u, v \in V_\ell, \\ \mathcal{A}_\ell : X_\ell &\rightarrow X_\ell & (\mathcal{A}_\ell u, v) &= \mathcal{A}_\ell(u, v) & \forall x, y \in X_\ell. \end{aligned}$$

3.6 Overlapping Schwarz Smoothers

In this section, we define a class of smoothing operators \mathcal{B}_ℓ used in the multi-grid V-cycle [51]. These smoothers are based on a subspace decomposition of the space X_ℓ corresponding to the overlapping subdomains of the triangulation \mathcal{T}_ℓ . We create the subdomains $\mathcal{T}_{\ell,\nu}$ in form of vertex patches in such a way that every subdomain contains all cells sharing the same vertex ν (See Fig: 3.1). In this way we get an overlapping covering with $N_\ell > 0$ patches, denoted by $\{\Omega_{\ell,\nu}\}_{\nu=1}^{N_\ell}$.

The subspace $X_{\ell,\nu} = V_{\ell,\nu} \times Q_{\ell,\nu}$ consists of the functions in X_ℓ with support in $\Omega_{\ell,\nu}$. This implies homogeneous slip boundary conditions on $\partial\Omega_{\ell,\nu}$ for the velocity subspace $V_{\ell,\nu}$ and zero mean value on $\Omega_{\ell,\nu}$ for the pressure space $Q_{\ell,\nu}$.

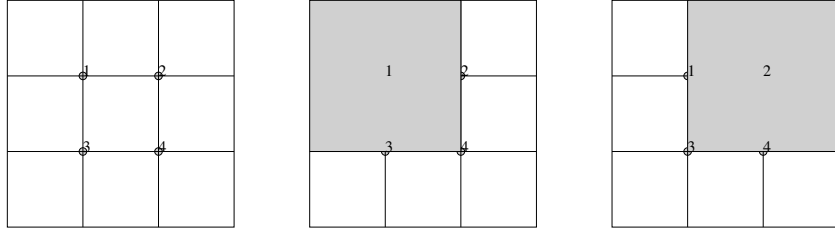


Figure 3.1: Subdomains consisting of vertex patches

3.6.1 Projection Operators

In this section, we describe some operators for interpolation and restriction. These operators will be used throughout this thesis for Schwarz smoothers. We assume the existence of restriction and interpolation operators as given in [71]. We suppose these operators for both, singularly perturbed problem and mixed form, as follows:

$$\begin{aligned} R_{\ell,\nu} : V_\ell &\longrightarrow V_{\ell,\nu}, & \mathcal{R}_{\ell,\nu} : X_\ell &\longrightarrow X_{\ell,\nu}, \\ R_{\ell,\nu}^T : V_{\ell,\nu} &\longrightarrow V_\ell, & \mathcal{R}_{\ell,\nu}^T : X_{\ell,\nu} &\longrightarrow X_\ell. \end{aligned}$$

Let us suppose the following decomposition of V_ℓ and X_ℓ

$$V_\ell = \sum_{\nu \in N_\ell} R_{\ell,\nu}^T V_{\ell,\nu}, \quad X_\ell = \sum_{\nu \in N_\ell} \mathcal{R}_{\ell,\nu}^T X_{\ell,\nu}.$$

When the space at level ℓ is decomposed as above then the representation of the any element of spaces (V_ℓ and X_ℓ) as the sum of elements of subspaces

$(V_{\ell,\nu}$ and $X_{\ell,\nu}$) is not unique.

For the subspaces, we introduce the local bilinear forms and matrices associated with them in the following way:

$$\begin{aligned} A_{\ell,\nu}(\cdot, \cdot) : V_{\ell,\nu} \times V_{\ell,\nu} &\longrightarrow \mathbb{R}, & \mathcal{A}_{\ell,\nu}(\cdot, \cdot) : X_{\ell,\nu} \times X_{\ell,\nu} &\longrightarrow \mathbb{R}, \\ A_{\ell,\nu} : V_{\ell,\nu} &\longrightarrow V_{\ell,\nu}, & \mathcal{A}_{\ell,\nu} : X_{\ell,\nu} &\longrightarrow X_{\ell,\nu}. \end{aligned}$$

These local bilinear forms can be different from the original global bilinear forms. However, in case of using the exact subspace solvers the local bilinear forms are inherited from the global form as following

$$\begin{aligned} A_{\ell,\nu}(u_\nu, v_\nu) &= A_\ell(R_{\ell,\nu}^T u_\nu, R_{\ell,\nu}^T v_\nu) \quad \forall u_\nu, v_\nu \in V_{\ell,\nu}, \\ \mathcal{A}_{\ell,\nu}(x_\nu, y_\nu) &= \mathcal{A}_\ell(\mathcal{R}_{\ell,\nu}^T x_\nu, \mathcal{R}_{\ell,\nu}^T y_\nu) \quad \forall x_\nu, y_\nu \in X_{\ell,\nu}, \end{aligned}$$

we get the following relations.

$$A_{\ell,\nu} = R_{\ell,\nu} A_\ell R_{\ell,\nu}^T, \quad \mathcal{A}_{\ell,\nu} = \mathcal{R}_{\ell,\nu} \mathcal{A}_\ell \mathcal{R}_{\ell,\nu}^T.$$

We define projection-like operators $P_{\ell,\nu} : V_\ell \longrightarrow V_{\ell,\nu}$ and $\mathcal{P}_{\ell,\nu} : X_\ell \longrightarrow X_{\ell,\nu}$ such that

$$A_{\ell,\nu}(P_{\ell,\nu} u_\ell, v_{\ell,\nu}) = A_\ell(u_\ell, R_{\ell,\nu}^T v_{\ell,\nu}) \quad \forall v_{\ell,\nu} \in V_{\ell,\nu}, \quad (3.8)$$

$$\mathcal{A}_{\ell,\nu}(\mathcal{P}_{\ell,\nu} x_\ell, y_{\ell,\nu}) = \mathcal{A}_\ell(x_\ell, \mathcal{R}_{\ell,\nu}^T y_{\ell,\nu}) \quad \forall y_{\ell,\nu} \in X_{\ell,\nu}. \quad (3.9)$$

By this definition we obtain a relation between local and global bilinear forms on level ℓ

$$A_{\ell,\nu} P_{\ell,\nu} = R_{\ell,\nu} A_\ell, \quad (3.10)$$

$$\mathcal{A}_{\ell,\nu} \mathcal{P}_{\ell,\nu} = \mathcal{R}_{\ell,\nu} \mathcal{A}_\ell. \quad (3.11)$$

3.6.2 Multiplicative Schwarz

To define the multiplicative Schwarz smoother, we start with the following multiplicative algorithm as given in [15].

Algorithm 3.6.1. *Given $u_\ell^i \in V_\ell$ is initial solution, we define the next iterate $u_\ell^{i+1} \in V_\ell$ as follows:*

1. $w_0 = u_\ell^i$.
2. For $\nu = 1, \dots, N_\ell$ define w_ν by

$$w_\nu = w_{\nu-1} + A_{\ell,\nu} R_{\ell,\nu} (f - A_\ell w_{\nu-1}).$$

3. Set $u_\ell^{i+1} = w_{N_\ell}$.

Let $E_0 = u_\ell - w_0$ and $E_\nu = u_\ell - w_\nu$ for $\nu = 1, \dots, N_\ell$. In addition we have the following relation in local to global forms

$$R_{\ell,\nu} A_\ell = A_{\ell,\nu} P_{\ell,\nu}$$

where $P_{\ell,\nu}$ is the projection operator defined in (3.10). So we can write the error propagation operator in the recursive form

$$E_\nu = (I - P_{\ell,\nu}) E_{\nu-1}$$

Consequently,

$$u_\ell - u_\ell^{i+1} = (I - P_{N_\ell})(I - P_{N_\ell-1}) \cdots (I - P_1)(u_\ell - u_\ell^i),$$

We define the symmetric multiplicative Schwarz smoother B_ℓ using the error propagation operators, associated with spaces $V_{\ell,\nu}$, by

$$B_\ell = (I - E_\ell^* E_\ell) A_\ell^{-1} \quad \text{with} \quad E_\ell = (I - P_{\ell,1}) \cdots (I - P_{\ell,N_\ell}), \quad (3.12)$$

where E_ℓ^* is the A_ℓ -adjoint of E_ℓ . Similarly the symmetric multiplicative Schwarz smoother \mathcal{B}_ℓ can be defined using the error propagation operators for mixed form, associated with spaces $X_{\ell,\nu}$, by

$$\mathcal{B}_\ell = (\mathcal{I} - \mathcal{E}_\ell^* \mathcal{E}_\ell) \mathcal{A}_\ell^{-1} \quad \text{with} \quad \mathcal{E}_\ell = (\mathcal{I} - \mathcal{P}_{\ell,1}) \cdots (\mathcal{I} - \mathcal{P}_{\ell,N_\ell}), \quad (3.13)$$

where \mathcal{E}_ℓ^* is the \mathcal{A}_ℓ -adjoint of \mathcal{E}_ℓ .

3.6.3 Convergence Analysis

In this section, we provide an overview of the convergence analysis of the Multiplicative Schwarz smoothers which has been presented in [15] and [79] as iterative methods. Here, we analyze these iterative methods as smoothers in the multigrid framework. In our analysis, we always use the exact solvers for the subspace problems which is different in the sense that they considered the approximation on the subproblems.

For convenience, we drop out the subscript ℓ in this section until it is necessary to use. For proving the convergence of the multiplicative algorithm we need to show that error reduces in each iteration which means we have the following contraction property

$$\|E\|_A \leq \delta \quad \text{where} \quad \|E\|_A = \sup_{u \in V} \frac{A(Eu, Eu)}{A(u, u)},$$

with a constant $0 < \delta < 1$. Here E is given in (3.12). As $E^*E = I - BA$, so we can also write this contraction property in the following form.

$$A((I - BA)u, u) \leq \delta^2 A(u, u) \quad \forall u \in V.$$

We have the following assumptions at hand for the analysis of these smoothers. Constant appearing in these assumptions determine an upper for contraction

as we will see later.

Stable Decomposition: For any $u \in V$ there exists a decomposition $u = \sum_{\nu=1}^N R_\nu^T u_\nu$ for $u_\nu \in V_\nu$, such that

$$\sum_{\nu=1}^N A_\nu(u_\nu, u_\nu) \leq C_0 A(u, u). \quad (3.14)$$

Strengthened Cauchy-Schwarz: There exist constants $0 \leq \epsilon_{\nu\xi} \leq 1, 1 \leq \nu, \xi \leq N$, such that

$$|A(R_\nu^T u_\nu, R_\xi^T u_\xi)| \leq \epsilon_{\nu\xi} A(R_\nu^T u_\nu, R_\nu^T u_\nu)^{1/2} A(R_\xi^T u_\xi, R_\xi^T u_\xi)^{1/2}, \quad (3.15)$$

for $u_\nu \in V_\nu$ and $u_\xi \in V_\xi$. We will denote the spectral radius of $\varepsilon = \{\epsilon_{\nu\xi}\}$ by $\rho(\varepsilon)$.

Local Stability: There exists a constant $\omega > 0$, such that

$$A(R_\nu^T u_\nu, R_\nu^T u_\nu) \leq \omega A_\nu(u_\nu, u_\nu), \quad u_\nu \in V_\nu, \quad 1 \leq \nu \leq N. \quad (3.16)$$

We present here a technical lemma which will be used in the main result for the convergence.

Lemma 3.6.1. *Denote for $1 \leq \nu \leq N$, $E_\nu = (I - P_\nu)(I - P_{\nu-1}) \cdots (I - P_1)$ and $E_0 = I$. Then*

$$I - E_\nu = \sum_{j=1}^{\nu} P_j E_{j-1}, \quad (3.17)$$

$$(2 - \omega) \sum_{\nu=1}^N A(P_\nu E_{\nu-1} v, E_{\nu-1} v) \leq A(v, v) - A(Ev, Ev) \quad \forall v \in V. \quad (3.18)$$

Proof. From the representation of E_ν we have the following identity

$$E_{\nu-1} - E_\nu = P_\nu E_{\nu-1},$$

which implies (3.17). Furthermore, we can deduce that

$$\begin{aligned}
A(E_{\nu-1}u, E_{\nu-1}u) - A(E_{\nu}u, E_{\nu}u) &= A(P_{\nu}E_{\nu-1}u, P_{\nu}E_{\nu-1}u) + 2A(P_{\nu}E_{\nu-1}u, E_{\nu}u), \\
&= A(P_{\nu}E_{\nu-1}u, P_{\nu}E_{\nu-1}u) + 2(P_{\nu}(I - P_{\nu})E_{\nu-1}u, E_{\nu-1}u), \\
&= ((2I - P_{\nu})P_{\nu}E_{\nu-1}u, E_{\nu-1}u), \\
&\geq (2 - \omega)(P_{\nu}E_{\nu-1}u, E_{\nu-1}u).
\end{aligned}$$

Summing up these inequalities over ν , gives (3.18). \square

In Lemma 3.6.1, the constant $\omega \in (0, 2)$ is the same constant which appears in the assumption of local stability. Now, we present a theorem which is main part of convergence analysis.

Theorem 3.6.1. *For the multiplicative algorithm, we have the following estimate*

$$A((I - BA)u, u) \leq \delta A(u, u) \quad \forall u \in V,$$

where $\delta = 1 - \frac{2-\omega}{C_0(1+C_1)^2}$.

Proof. The proof of this theorem is presented in ([79], Theorem 4.4) which can be followed for exact subspace solvers as here is the case. \square

We see from this theorem the contraction constant depends on the constants ω , C_0 and C_1 . For estimates of constants, we start with the constant $\omega \in (0, 2)$ which appears in local stability estimate and is one in case of the exact subspace solvers. C_0 is the constant from stable decomposition and C_1 depends on the spectral radius $\rho(\varepsilon)$ corresponding the strengthened Cauchy-Schwarz inequality.

3.7 Multigrid preconditioner

In this section, we describe our method for building multigrid preconditioners and their convergence analysis for symmetric problems. As described in Section 2.2, we use multi-level meshes. By having these multi-level meshes, which contain nested mesh cells, we have the nestedness of finite element spaces as follows:

$$\begin{aligned} V_0 &\subset V_1 \subset \dots \subset V_L, \\ Q_0 &\subset Q_1 \subset \dots \subset Q_L, \\ X_0 = V_0 \times Q_0 &\subset X_1 \subset \dots \subset V_L \times Q_L = X_L. \end{aligned}$$

This relation extends to the divergence free subspaces, see [52]

$$V_0^0 \subset V_1^0 \subset \dots \subset V_L^0. \quad (3.19)$$

3.7.1 Projection Operators

The nestedness of the spaces implies that there is a sequence of operators $\mathcal{I}_\ell^T : X_\ell \rightarrow X_{\ell+1}$ of the form $\mathcal{I}^T(v_\ell, q_\ell) = (I_{\ell,u}^T v_\ell, I_{\ell,p}^T q_\ell)$, such that

$$I_{\ell,u}^T : V_\ell \rightarrow V_{\ell+1}, \quad I_{\ell,p}^T : Q_\ell \rightarrow Q_{\ell+1}, \quad (3.20)$$

$$I_{\ell,u}^T : V_\ell^0 \rightarrow V_{\ell+1}^0. \quad (3.21)$$

The L^2 -projection of $\mathcal{I}_\ell : X_{\ell+1} \rightarrow X_\ell$ is defined by

$$\mathcal{I}_\ell(v_\ell, q_\ell) = (I_{\ell,u} v_\ell, I_{\ell,p} q_\ell),$$

with

$$(v_{\ell+1} - I_{\ell,u}v_{\ell+1}, w_\ell) = 0 \quad \forall w_\ell \in V_\ell \quad (q_{\ell+1} - I_{\ell,p}q_{\ell+1}, r_\ell) = 0 \quad \forall r_\ell \in Q_\ell. \quad (3.22)$$

The \mathcal{A} -orthogonal projection \mathcal{P} from $(V_{\ell+1} \times Q_{\ell+1}) \rightarrow (V_\ell \times Q_\ell)$ is defined by

$$\mathcal{A}_\ell \left(\mathcal{P}_\ell \begin{pmatrix} u_{\ell+1} \\ p_{\ell+1} \end{pmatrix}, \begin{pmatrix} v_\ell \\ p_\ell \end{pmatrix} \right) = \mathcal{A}_{\ell+1} \left(\begin{pmatrix} u_{\ell+1} \\ p_{\ell+1} \end{pmatrix}, \mathcal{I}_\ell^T \begin{pmatrix} v_\ell \\ p_\ell \end{pmatrix} \right), \quad (3.23)$$

for all $(u_{\ell+1}, p_{\ell+1}) \in (V_{\ell+1} \times Q_{\ell+1})$ and $(v_\ell, p_\ell) \in V_\ell \times Q_\ell$. Similarly, The \mathcal{A} -orthogonal projection P_ℓ from $V_{\ell+1} \rightarrow V_\ell$ is defined by

$$A_\ell(P_\ell u_{\ell+1}, v_\ell) = A_{\ell+1}(u_{\ell+1}, I_{\ell,u}^T v_\ell), \quad (3.24)$$

for all $u_{\ell+1} \in V_{\ell+1}, v_\ell \in V_\ell$. From these definitions of the projection operators, we have the following relationship between consecutive levels.

$$\mathcal{A}_\ell \mathcal{P}_\ell = \mathcal{I}_\ell \mathcal{A}_{\ell+1}, \quad A_\ell P_\ell = I_\ell A_{\ell+1}. \quad (3.25)$$

As, we have the multi-level structure of the spaces $V_\ell \times Q_\ell$, $\ell = 0, \dots, L$, so on each level ℓ we rewrite the weak formulation to find $(u_\ell, p_\ell) \in V_\ell \times Q_\ell$ such that

$$\mathcal{A}_\ell \left(\begin{pmatrix} u_\ell \\ p_\ell \end{pmatrix}, \begin{pmatrix} v_\ell \\ q_\ell \end{pmatrix} \right) = \begin{pmatrix} f \\ v_\ell \end{pmatrix} \quad \forall (v_\ell, q_\ell) \in V_\ell \times Q_\ell,$$

in algebraic form $\mathcal{A}_\ell x_\ell = b_\ell$ where $x_\ell \equiv \begin{pmatrix} u_\ell \\ p_\ell \end{pmatrix}$ and $b_\ell \equiv \begin{pmatrix} f \\ v_\ell \end{pmatrix}$ is the right hand side of the system.

3.7.2 V-cycle Algorithm

The multigrid preconditioner $\mathcal{M}_\ell : X_\ell \rightarrow X_\ell$, where $(X_\ell = V_\ell \times Q_\ell)$ is defined recursively in V-cycle with $m(\ell) \geq 1$ pre-smoothing and post-smoothing

steps. Let \mathcal{B}_ℓ be suitable smoother. We assume that the coarse mesh problem $\mathcal{A}_0 x_0 = b_0$ has a small size so that we directly invert \mathcal{A}_0 and have $\mathcal{M}_0 = \mathcal{A}_0^{-1}$. For $\ell \geq 1$, we define the action of \mathcal{M}_ℓ on vector $b_\ell \in X_\ell$ as follows:

- Pre-smoothing:

$$x_i = x_{i-1} + \mathcal{B}_\ell(b_\ell - \mathcal{A}_\ell x_{i-1}) \quad i = 1, \dots, m(\ell).$$

- Coarse grid correction:

$$x_{m(\ell)+1} = x_{m(\ell)} + \mathcal{I}_{\ell-1}^T \mathcal{M}_{\ell-1} \mathcal{I}_{\ell-1}(b_\ell - \mathcal{A}_\ell x_{m(\ell)}).$$

- Post-smoothing:

$$x_i = x_{i-1} + \mathcal{B}_\ell(b_\ell - \mathcal{A}_\ell x_{i-1}) \quad i = m(\ell) + 2, \dots, 2m(\ell) + 1.$$

- Assign:

$$\mathcal{M}_\ell b_\ell = x_{2m(\ell)+1}.$$

The number of smoothing steps $m(L)$ on the finest level is a free parameter and for the standard V-cycle $m(\ell) = m(L)$, whereas in the case of variable V-cycle, this becomes $m(\ell) = m(L)2^{L-\ell}$. The smoothers \mathcal{B}_ℓ are overlapping Schwarz smoothers discussed in Section (3.6). We refer to \mathcal{M}_L as the V-cycle preconditioner of \mathcal{A} . The V-cycle iteration is given by

$$x_{k+1} = x_k + \mathcal{M}_L(b_L - \mathcal{A}_L x_k). \quad (3.26)$$

The definition of the preconditioner $M_\ell : V_\ell \longleftrightarrow V_\ell$ for the elliptic operator A_ℓ follows the same concept, but dropping the pressure variables.

3.7.3 Recurrence Relation

We derive a recurrence relation for the error operator $I - M_\ell \mathcal{A}_\ell$ of the V-cycle algorithm as given in [14]. This operator will be used in the following convergence analysis. After $m(\ell)$ smoothing steps, we have

$$x - x_{m(\ell)} = \mathcal{K}_\ell^{m(\ell)} x, \quad \mathcal{K}_\ell^{m(\ell)} = (I - \mathcal{B}_\ell \mathcal{A}_\ell)^{m(\ell)}.$$

Then from the correction step, it follows:

$$x - x_{m(\ell)+1} = x - x_{m(\ell)} - \mathcal{M}_{\ell-1} \mathcal{I}_{\ell-1} \mathcal{A}_\ell (x - x_{m(\ell)}),$$

where $b_\ell = \mathcal{A}_\ell x$. By using the relation given in (3.25), we get

$$\begin{aligned} x - x_{m(\ell)+1} &= (I - \mathcal{M}_{\ell-1} \mathcal{A}_{\ell-1} \mathcal{P}_{\ell-1})(x - x_{m(\ell)}), \\ &= (I - \mathcal{M}_{\ell-1} \mathcal{A}_{\ell-1} \mathcal{P}_{\ell-1}) \mathcal{K}_\ell^{m(\ell)} x, \end{aligned} \tag{3.27}$$

and finally we have the following relation

$$\begin{aligned} (I - \mathcal{M}_\ell \mathcal{A}_\ell)x &= x - x_{2m(\ell)} - \mathcal{B}_\ell \mathcal{A}_\ell (x - x_{2m(\ell)}), \\ &= \mathcal{K}_\ell^{m(\ell)} (x - x_{m(\ell)+1}), \\ &= \mathcal{K}_\ell^{m(\ell)} (I - \mathcal{M}_{\ell-1} \mathcal{A}_{\ell-1} \mathcal{P}_{\ell-1}) \mathcal{K}_\ell^{m(\ell)} x, \end{aligned}$$

since $x \in X_\ell$ is arbitrary. Hence, we have

$$(I - \mathcal{M}_\ell \mathcal{A}_\ell) = \mathcal{K}_\ell^{m(\ell)} (I - \mathcal{M}_{\ell-1} \mathcal{A}_{\ell-1} \mathcal{P}_{\ell-1}) \mathcal{K}_\ell^{m(\ell)}, \tag{3.28}$$

$$= \mathcal{K}_\ell^{m(\ell)} [(I - \mathcal{P}_{\ell-1}) + (I - \mathcal{M}_{\ell-1} \mathcal{A}_{\ell-1}) \mathcal{P}_{\ell-1}] \mathcal{K}_\ell^{m(\ell)}. \tag{3.29}$$

3.7.4 Convergence Analysis

In this section, we give an overview of the convergence analysis for multigrid preconditioner with overlapping Schwarz smoothers. Most of the results are part of the standard multigrid theory. The detailed analysis on the convergence of multigrid has been done by Kanschat and Mao [52] for Stokes problem. Here, we skip proofs of theorems and only present some results related to convergence of multigrid method. This shows that multigrid method is independent of mesh parameters. For detailed proofs and discussion, we refer to [52] and [59]. The main result is presented in form of following theorem.

Theorem 3.7.1. *The multilevel iteration $\mathcal{I} - \mathcal{M}_L \mathcal{A}_L$ for the Stokes problem with the variable V-cycle operator defined in Section 3.7.2 employing the smoother \mathcal{B}_ℓ defined in (3.12) is a contraction with contraction number independent of the mesh level ℓ .*

To prove this theorem, first they proved the same result for singularly perturbed problem as described in Section 3.5. Then they have the following result for the equivalence between mixed problem and singularly perturbed problem.

Theorem 3.7.2. *The multigrid algorithm in mixed variables preserves the space $X_{\ell,\epsilon}$. On this subspace it is equivalent to the multigrid algorithm in primal variables. This means for $(u_\ell, p_\ell) \in X_{\ell,\epsilon}$ and $(\hat{u}_\ell, \hat{p}_\ell) = \mathcal{M}_\ell(u_\ell, p_\ell)$ there holds $(\hat{u}_\ell, \hat{p}_\ell) \in X_{\ell,\epsilon}$ and*

$$\hat{u}_\ell = M_\ell u_\ell,$$

where \mathcal{M}_ℓ and M_ℓ are the corresponding multigrid operators for each algorithm.

In theoretical perspective these results are only proved for symmetric positive definite systems. For proving these results, they used the recurrence relation given in (3.28) and (3.29) and the symmetry of the system.

3.7.5 Downwind Ordering

We extend multigrid methods with Schwarz smoothers to non-symmetric problems by incorporating the downwind ordering of Bey[12] and Hackbusch[37]. We apply this sorting scheme to the vertices of the mesh because we use vertex patches as our subdomains in Schwarz methods for smoothing. This downwind ordering of vertex patches is effective when the convection direction is constant which means there are no cycles in flow. Otherwise, when there are vortices in flow then simple sorting in downwind direction is not sufficient alone. In those cases, we consider sorting in multiple directions, known as full sweep. In computational results, we have observed that in case of convection dominated flows (high Reynolds number) downwind ordering is considerably effective and we get the iterations count for linear solver those are comparable to Laplace problem.

3.8 Numerical Results

We test multigrid preconditioners with overlapping Schwarz smoothers for the Oseen problem. For our tests, we consider the following two dimensional

analytical solutions as the exact solutions for the computing errors and convergence rates.

Remark 3.8.1. *We implemented all of our solvers in C++ by using a finite element library **deal.II**[11, 7]. All the computational results in later chapters are also obtained by using the same library.*

Remark 3.8.2. *For all of our results, there is only one cell in the coarse mesh such that $T = \Omega$. On a finer level ℓ the mesh is obtained by dividing all the cells on coarser level $\ell - 1$ into four cells so that the mesh on level ℓ has 4^ℓ cells.*

3.8.1 Poiseuille Flow

The Poiseuille flow of incompressible fluid a pipe or channel is modeled by Navier-Stokes equations. The solution can be described, in terms of Reynolds number Re , as following.

$$\begin{aligned} u_1(x, y) &= 1 - \frac{1}{L^2} (x^2 + y^2), \\ u_2(x, y) &= 0, \\ p(x, y) &= -\frac{1}{L^2} \frac{2x}{Re} + C, \end{aligned} \tag{3.30}$$

where a constant C is chosen in such a way that $\int_{\Omega} p d\mathbf{x} = 0$. The Reynolds number is defined as $Re = \frac{UL}{\nu}$, where U is the velocity of the fluid and L is characteristic length. In our case characteristic length is radius of channel. We take the domain $\Omega = (-1, 1)^2$ with non-homogeneous Dirichlet boundary conditions, where the velocities at boundary of domain are give by (3.30). By choosing $\beta = u$ and $\gamma = 0$, the functions given in (3.30) solve the equation

(3.1).

In Table 3.1, the convergence rates for errors are presented for finite element spaces pair $RT_1 \times Q_1$ and $\nu = 10^{-2}$. Reduction of residual is set to 10^{-10} . We observe optimal convergence of L^2 and H^1 errors for both velocity and pressure.

Levels	$\ u - u_h\ _{L^2}$		$\ u - u_h\ _{H^1}$		$\ p - p_h\ _{L^2}$		$\ p - p_h\ _{H^1}$	
3	3.8515e-02	-	5.8002e-01	-	4.6650e-03	-	1.5503e-02	-
4	9.7420e-03	1.98	2.8928e-01	1.00	1.3147e-03	1.83	6.2433e-03	1.31
5	2.4967e-03	1.96	1.4449e-01	1.00	3.7782e-04	1.80	2.6985e-03	1.21
6	6.4058e-04	1.96	7.2216e-02	1.00	1.0326e-04	1.87	1.2541e-03	1.11
7	1.6318e-04	1.97	3.6098e-02	1.00	2.7518e-05	1.91	6.1207e-04	1.03
8	4.1264e-05	1.98	1.8046e-02	1.00	7.2233e-06	1.93	3.0396e-04	1.01

Table 3.1: Convergence rates of errors for Poiseuille flow

3.8.2 Kovaszny Flow

Another two dimensional analytical solution of incompressible Navier-Stokes equations is derived by Kovaszny [57] which can be described by Reynolds number Re in terms of parameter $\lambda = Re/2 - \sqrt{Re^2/4 + 4\pi^2}$.

$$\begin{aligned}
 u_1(x, y) &= 1 - \exp^{\lambda x} \cos 2\pi y, \\
 u_2(x, y) &= \frac{\lambda}{2\pi} \exp^{\lambda x} \sin 2\pi y, \\
 p(x, y) &= \frac{1}{2} \exp^{2\lambda x} + C.
 \end{aligned} \tag{3.31}$$

Where we choose the constant C such that mean pressure is $\int_{\Omega} p d\mathbf{x} = 0$. We consider the domain in this case $\Omega = (-\frac{1}{2}, \frac{3}{2}) \times (0, 2)$ with inhomogeneous

Dirichlet boundary conditions in which the velocities are given by (3.31). In this test case, we choose $\beta = u$ and $\gamma = 0$ which satisfy the condition (3.2). Therefore, the analytical solution given in (3.31) satisfies (3.1). In Figure 3.2, we show that the Kovaszny flow problem is rather difficult to solve as we observe a reverse flow from the stream line representation of velocity. Here the color scale from red to blue shows high to low speeds respectively. The analytical solution in (3.31) is smooth for any Reynolds number which allows us to test our method for the higher order elements and any Reynolds number. Thus in Table 3.2, k is the degree of polynomial used in the finite element pair $RT_k \times Q_k$ and we can observe the optimal convergence rates of L^2 and H^1 errors of velocity and pressure. These results are obtained to reduce the residual to 10^{-10} for Reynolds number $Re = 10$.

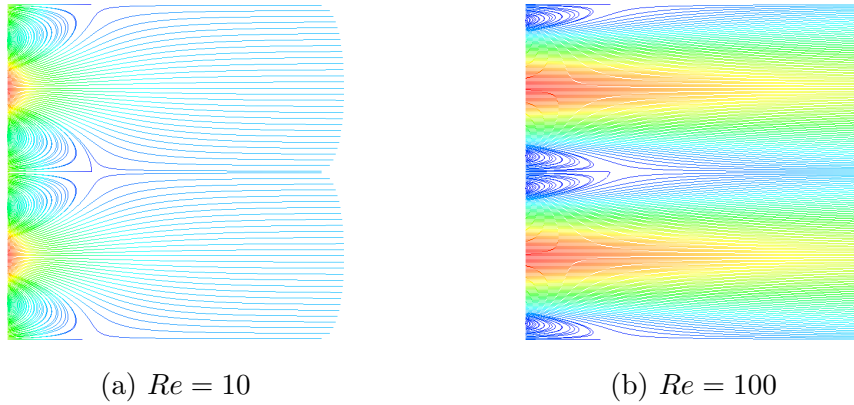


Figure 3.2: Velocity stream lines for Kovaszny flow

k	ℓ	$\ u - u_h\ _{L^2}$		$\ u - u_h\ _{H^1}$		$\ p - p_h\ _{L^2}$		$\ p - p_h\ _{H^1}$	
1	5	5.6000e-02	1.88	2.6585e+00	1.00	1.1640e-01	1.76	5.6070e+00	0.90
	6	1.4541e-02	1.95	1.3270e+00	1.00	3.3487e-02	1.80	2.8676e+00	0.97
	7	3.7279e-03	1.96	6.6286e-01	1.00	9.4132e-03	1.83	1.4424e+00	0.99
2	5	3.6596e-03	2.99	2.7714e-01	1.99	1.0209e-02	2.60	7.1736e-01	1.73
	6	4.5875e-04	3.00	6.8776e-02	2.01	1.6827e-03	2.60	2.1249e-01	1.76
	7	5.7358e-05	3.00	1.7120e-02	2.01	2.8395e-04	2.57	6.5361e-02	1.70
3	5	2.0577e-04	3.84	1.8446e-02	3.01	6.6551e-04	3.50	6.5624e-02	2.66
	6	1.3806e-05	3.90	2.2682e-03	3.02	6.8288e-05	3.28	1.0231e-02	2.68
	7	8.8572e-07	3.95	2.8037e-04	3.02	4.8829e-06	3.54	1.6580e-03	2.63

Table 3.2: Convergence rates of errors for Kovasznay flow

3.8.3 Multigrid Performance

We carried out all of numerical tests for flow problems as mentioned above, with multigrid preconditioner using multiplicative Schwarz smoothers. In (3.1), we have both the diffusion term and convection term. Hence, we perform our numerical tests for low and high Reynolds number: diffusion dominated case and convection dominated case. We have observed that with multiplicative smoothers sorting of the vertex patches in direction of flow improves the result as presented in Table 3.3. Where vertex patches are the overlapping subdomains used in the building Schwarz smoothers. Sorting is considerably effective in case of convection dominated problems as the flow of information follows the direction of flow. Therefore sorting in the direction of flow reduces the number of iteration of the linear solver quite notably which can be seen in Table 3.3 in which we present the number of GMRES iterations

level	$\nu = 10^{-2}$		$\nu = 10^{-3}$		$\nu = 10^{-4}$	
	sorted	non-sorted	sorted	non-sorted	sorted	non-sorted
3	4	4	5	5	5	5
4	4	5	7	10	8	13
5	6	9	6	14	10	26
6	7	10	6	18	12	55
7	8	10	7	35	11	fails
8	8	10	7	42	11	fails

Table 3.3: GMRES iterations for variation of parameter ν with and without sorting

to reduce the residual to 10^{-6} for different diffusion coefficients. Both cases with sorting and without sorting are included to make a comparison. For these results we used the finite element spaces pair $RT_1 \times Q_1$ which is also the case for following tables if not otherwise mentioned.

In Tables 3.4 and 3.5, we present the iteration count for a variety of Reynolds number in case of using one and two smoothing steps respectively. In these tables, the results are for Poisseuille flow function. We observed that the number of GMRES iterations is independent of mesh parameter and Reynolds number. Similarly, in Tables 3.6 and 3.7, the iteration count in case of Kovasznay flow function is presented for one and two smoothing steps for different Reynolds number. Observation in this case is that the number of GMRES iterations is independent of the mesh parameters but it starts increasing after a certain limit of Reynolds number. These results show

	<i>ReynoldsNumbers</i>							
levels	1.0	10.0	50.0	100.0	500.0	1000.0	5000.0	10000.0
3	5	4	3	4	4	5	5	5
4	6	6	5	4	5	7	8	8
5	7	7	6	6	5	6	10	10
6	7	7	7	7	6	6	9	12
7	7	8	8	8	7	7	9	11
8	7	8	9	8	7	7	8	11

Table 3.4: Iteration count for different Reynolds numbers using $RT_1 \times Q_1$ for Poiseuille flow function with $m(\ell) = 1$

	<i>ReynoldsNumbers</i>							
levels	1.0	10.0	50.0	100.0	500.0	1000.0	5000.0	10000.0
3	4	3	3	3	3	3	3	3
4	5	5	4	4	4	5	6	6
5	5	5	6	5	4	4	7	8
6	5	5	6	6	5	5	6	8
7	5	5	6	6	5	5	5	7
8	5	5	6	6	5	5	5	5

Table 3.5: Iteration count for different Reynolds numbers using $RT_1 \times Q_1$ for Poiseuille flow function with $m(\ell) = 2$

the efficiency of the multigrid precondition in case of convection dominated problems when multiplicative Schwarz smoothers are used with sorting of vertex patches in convection direction.

	<i>ReynoldsNumbers</i>							
levels	1.0	10.0	50.0	100.0	500.0	1000.0	5000.0	10000.0
3	4	4	4	4	5	5	5	5
4	6	6	5	5	6	7	8	9
5	6	7	7	6	6	8	11	11
6	7	7	8	7	7	7	13	15
7	7	8	8	8	8	8	12	17
8	7	8	9	9	8	8	12	15

Table 3.6: Iteration count for different Reynolds numbers using $RT_1 \times Q_1$ for Kovasznay flow function with $m(\ell) = 1$

In Table 3.8, we present the iteration count for different relaxation parameter which is used in the multiplicative Schwarz smoother. We perform these tests for the choice of optimal relaxation parameter. As we can see from these numbers that $r = 1.0$ is suitable choice for the relaxation parameter in this case which may not be optimal for the case of additive smoothers. These numbers are required to reduce the residual by 10^{-6} by using finite element pair $RT_1 \times Q_1$ and for Reynolds number $Re = 100$. We have presented mostly the iteration counts by using only first order Raviart-Thomas element for the variation of other parameters. In Table 3.9, we tabulate the iteration count for different polynomial degrees used in the finite element

	<i>ReynoldsNumbers</i>							
levels	1.0	10.0	50.0	100.0	500.0	1000.0	5000.0	10000.0
4	4	4	4	4	5	5	5	6
5	5	5	6	5	4	5	7	8
6	5	5	6	6	5	5	9	10
7	5	5	6	6	5	5	7	10
8	5	5	6	6	5	5	7	9
9	13	5	6	6	6	5	5	6

Table 3.7: Iteration count for different Reynolds numbers using $RT_1 \times Q_1$ for Kovaszny flow function with $m(\ell) = 2$

level	Iterations		
	$r = 1.0$	$r = 0.7$	$r = 0.5$
3	4	4	6
4	4	5	7
5	6	6	8
6	7	7	9
7	8	8	9
8	8	8	9

Table 3.8: Number of iterations for different relaxation parameters

pair $RT_k \times Q_k$ for two different Reynolds numbers. Figures in this table show that the multigrid method is robust with respect to polynomial degree

and Reynolds number.

In Table 3.10, we present a comparison of multigrid preconditioners with

	$\nu = 10^{-1}$					$\nu = 10^{-3}$				
levels	$k = 1$	$k = 2$	$k = 3$	$k = 4$	$k = 5$	$k = 1$	$k = 2$	$k = 3$	$k = 4$	$k = 5$
3	4	4	3	3	3	5	4	3	3	3
4	6	4	4	4	3	7	4	4	3	3
5	7	4	4	4	3	6	4	4	3	3
6	7	4	4	4	3	6	4	4	4	4
7	8	4	4	4	3	7	4	4	4	4

Table 3.9: GMRES iterations for FE pair $RT_k \times Q_k$

block preconditioners. Where Tables 3.10b and 3.10a shows the numbers from [35, 55] for Poiseuille flow using block preconditioners and in Table 3.10c, we tabulate the iteration count for multigrid preconditioner. We observe that multigrid preconditioners are much more efficient as compared to the block preconditioners. Here, we see a slightly higher number in iteration counts for multigrid preconditioner as compare to our previous results. It is because of a more stringent stopping criterion. As these iteration numbers are for GMRES to reduce the residual by a factor of 10^{10} which was also used in [35, 55].

	ν		
levels	10^{-2}	10^{-3}	10^{-4}
3	44	119	377
4	39	137	1183
5	39	110	945
6	42	71	774
7	48	50	397

	ν		
levels	10^{-2}	10^{-3}	10^{-4}
3	59	181	440
4	56	201	1129
5	55	134	1226
6	59	107	964
7	66	82	615

(a) Block preconditioners Kay/Loghin

(b) Block preconditioners Kanschat

	ν		
levels	10^{-2}	10^{-3}	10^{-4}
3	5	8	8
4	7	10	13
5	9	10	17
6	12	10	20
7	14	12	19

(c) Multigrid preconditioner

Table 3.10: Comparison of multigrid preconditioners with block preconditioners

3.9 Summary

In this chapter, we have mostly presented numerical results for the Oseen equations using multigrid preconditioners employing overlapping Schwarz smoothers of multiplicative type. We discretized the Oseen equations by

H^{div} -conforming discontinuous elements. The linear systems arising from discretization are non-symmetric systems and there is not enough theory of multigrid methods for non-symmetric problems. Hence, we presented an overview of multigrid theory for symmetric problems and we have performed our numerical experiments in view of this theory. We observed that multigrid preconditioners efficient as compared to the block preconditioners and robustness with respect the mesh size, the Reynolds number and the polynomial degree is shown by empirical results.

Chapter 4

The Navier-Stokes Equations

4.1 Introduction

In this chapter, we extend our numerical experiments to the Navier-Stokes equations to show the performance of multigrid method. The system is discretized with H^{div} -conforming discontinuous Galerkin method. Since, the Navier-Stokes equations are nonlinear, we use Picard iteration scheme as outer solver for non-linearity and GMRES, with multigrid preconditioner employing overlapping Schwarz smoothers, as inner solver for solving linear problems. Finally, we present numerical results for different fluid flow problems. We observe from our empirical results that multigrid preconditioners are efficient and robust for low Reynolds number with respect to the mesh size in a sense that iteration count for linear solver deteriorates slowly.

4.2 Model Problem

Consider the Navier-Stokes equations

$$\begin{aligned} -\nu\Delta u + (u \cdot \nabla) u + \nabla p &= \mathbf{f} && \text{in } \Omega, \\ \nabla \cdot u &= 0 && \text{in } \Omega, \\ u &= \mathbf{g} && \text{on } \partial\Omega, \end{aligned} \tag{4.1}$$

where u is the velocity, p the pressure, $\mathbf{f} \in L^2(\Omega)^d$ prescribed external body force and ν is the kinematic viscosity.

4.3 Discontinuous Galerkin discretization

In this section, we present the discretization of Navier-Stokes equations with discontinuous Galerkin method. This type of discretization has already been presented for the Oseen equations in Section 3.3. The Oseen equations are a linearized version of the Navier-Stokes equations. Hence, by considering the discretization of Oseen equations in compact form given in (3.3), we have the following DG discretization for Navier-Stokes equations in compact form.

$$a_\ell(u_\ell, v_\ell) + b_\ell(\beta; u_\ell, v_\ell) + (p_\ell, \nabla \cdot v_\ell) - (q_\ell, \nabla \cdot u_\ell) = (\mathbf{f}, v_\ell), \tag{4.2}$$

and

$$\beta = u, \tag{4.3}$$

for $v_\ell \in V_\ell$ and $q_\ell \in Q_\ell$. The definitions of the bilinear forms, for diffusion and convection terms, in (4.2) are same as given in section 3.3 for Oseen equations.

For non-linearity in convection term, we use an approach to separate the variables β and u rather than using equality in convection term. Then, we solve our non-linearity through fixed point iterations using (4.3). For the details of this approach, we refer to [22] and [21] where it is shown that this fixed point iteration is a contraction.

The discrete weak formulation of (4.1) reads now: find $(u_\ell, p_\ell) \in V_\ell \times Q_\ell$ such that for all test functions $v_\ell \in V_\ell$ and $q_\ell \in Q_\ell$ there holds

$$\mathcal{A}_\ell \left(\begin{pmatrix} u_\ell \\ p_\ell \end{pmatrix}, \begin{pmatrix} v_\ell \\ q_\ell \end{pmatrix} \right) = \mathcal{F}(v_\ell, q_\ell) \quad \forall v_\ell \in V_\ell, q_\ell \in Q_\ell, \quad (4.4)$$

where

$$\begin{aligned} \mathcal{A}_\ell \left(\begin{pmatrix} u_\ell \\ p_\ell \end{pmatrix}, \begin{pmatrix} v_\ell \\ q_\ell \end{pmatrix} \right) &\equiv a_\ell(u_\ell, v_\ell) + b_\ell(\beta; u_\ell, v_\ell) + (p_\ell, \nabla \cdot v_\ell) - (q_\ell, \nabla \cdot u_\ell), \\ \mathcal{F}(v_\ell, q_\ell) &\equiv (\mathbf{f}, v_\ell). \end{aligned}$$

4.4 Existence and Uniqueness of Solution

For showing the existence and uniqueness of discrete solution for DG discretization of Navier-Stokes equations, we follow the same approach as given in Section 3.4 for the Oseen equations. We recall that the DG norm is given as following:

$$\|u\|_\sigma^2 = \sum_{T \in \mathcal{T}_\ell} \|\nabla u\|_{L^2(T)}^2 + \sum_{F \in \mathcal{F}_\ell} \int_F \sigma_L |\llbracket u \otimes \mathbf{n} \rrbracket|^2 ds.$$

As we solve in each Picard iteration the Oseen system and we have already shown that there exists a unique solution for discretization of the Oseen

equations. Hence, in case of the Navier-Stokes equations we have additionally the smallness condition.

$$\mu := \frac{c_0 c_p \|\mathbf{f}\|_{L^2(\Omega)}}{\nu^2 \alpha^2} < 1.$$

Where $c_p > 0$ is constant independent of the mesh size appearing in the following Poincaré inequality

$$\|u_\ell\|_{L^2(\Omega)} \leq c_p \|u_\ell\| \quad \forall u_\ell \in V_\ell.$$

Theorem 4.4.1. *If $(u_\ell^{i+1}, p_\ell^{i+1})$ is the approximate solution given by DG discretization for the Oseen equations with $\beta = u_\ell^i, i \geq 0$, then*

$$\begin{aligned} \|u_\ell - u_\ell^{i+1}\| &\leq 2 \left(\frac{c_p \|\mathbf{f}\|_{L^2(\Omega)}}{\nu \alpha} \right) \frac{\mu^i}{(1 - \mu)}, \\ \|p_\ell - p_\ell^{i+1}\|_{L^2(\Omega)} &\leq 2\gamma_\ell^{-1} \left(\frac{c_a + 2\alpha}{\alpha} \right) c_p \|\mathbf{f}\|_{L^2(\Omega)} \frac{\mu^i}{(1 - \mu)}, \end{aligned}$$

for any initial guess $(u_\ell^0, p_\ell^0) \in V_\ell \times Q_\ell$.

Proof. See [21]. □

The smallness condition ensures the unique solution of 4.4 in addition with the above result for Picard iteration.

4.5 Overlapping Schwarz Smoothers

In this section, we present overlapping multiplicative Schwarz smoothers used for Navier-Stokes problem in preconditioning of linear solver with multi-grid preconditioner. We have given a detailed discussion on these type of

smoothers in Section 3.6, here we use the same smoothers but for Navier-Stokes problem. We define multiplicative Schwarz smoothers by using the following projection-like operator

$$\mathcal{A}_{\ell,\nu} \left(\mathcal{P}_{\ell,\nu} \begin{pmatrix} u_\ell \\ p_\ell \end{pmatrix}, \begin{pmatrix} v_{\ell,\nu} \\ q_{\ell,\nu} \end{pmatrix} \right) = \mathcal{A}_\ell \left(\begin{pmatrix} u_\ell \\ p_\ell \end{pmatrix}, \begin{pmatrix} v_{\ell,\nu} \\ q_{\ell,\nu} \end{pmatrix} \right) \quad \forall \begin{pmatrix} v_{\ell,\nu} \\ q_{\ell,\nu} \end{pmatrix} \in X_{\ell,\nu} \quad (4.5)$$

where $X_{\ell,\nu} = V_{\ell,\nu} \times Q_{\ell,\nu}$. The symmetric multiplicative Schwarz smoother \mathcal{B}_ℓ using the error propagation operators, associated with spaces $X_{\ell,\nu}$, are

$$\mathcal{B}_\ell = (\mathcal{I} - \mathcal{E}_\ell^* \mathcal{E}_\ell) \mathcal{A}_\ell^{-1} \quad \text{with} \quad \mathcal{E}_\ell = (\mathcal{I} - \mathcal{P}_{\ell,1}) \cdots (\mathcal{I} - \mathcal{P}_{\ell,N_\ell}) \quad (4.6)$$

where \mathcal{E}_ℓ^* is the \mathcal{A}_ℓ -adjoint of \mathcal{E}_ℓ .

For these smoothers, convergence analysis is part of standard theory in case of symmetric problems. There is very little theory for non-symmetric problems and almost no numerical results. We use the same setting for smoothers as given for symmetric problems and apply to our non-symmetric problem for numerical results.

4.6 Multigrid preconditioner

For building the multigrid preconditioners for Navier-Stokes problem, we adapt the same approach as described in Section 3.7. The multigrid preconditioner $\mathcal{M}_\ell : X_\ell \rightarrow X_\ell$ where $(X_\ell = V_\ell \times Q_\ell)$ is defined recursively in V-cycle with $m(\ell) \geq 1$ pre and post smoothing steps. Let \mathcal{B}_ℓ be suitable smoother. We assume that the coarse mesh problem $\mathcal{A}_0 x_0 = b_0$ has a small size so that we directly invert \mathcal{A}_0 and have $\mathcal{M}_0 = \mathcal{A}_0^{-1}$. For $\ell \geq 1$ define the action of \mathcal{M}_ℓ on vector $b_\ell \in X_\ell$:

- Pre-smoothing:

$$x_i = x_{i-1} + \mathcal{B}_\ell(b_\ell - \mathcal{A}_\ell x_{i-1}) \quad i = 1, \dots, m(\ell).$$

- Coarse grid correction:

$$x_{m(\ell)+1} = x_{m(\ell)} + \mathcal{I}_{\ell-1}^T \mathcal{M}_{\ell-1} \mathcal{I}_{\ell-1} (b_\ell - \mathcal{A}_\ell x_{m(\ell)}),$$

where \mathcal{I}_ℓ^T and \mathcal{I}_ℓ are the same operators as defined in section 3.7.1.

- Post-smoothing:

$$x_i = x_{i-1} + \mathcal{B}_\ell(b_\ell - \mathcal{A}_\ell x_{i-1}) \quad i = m(\ell) + 2, \dots, 2m(\ell) + 1.$$

- Assign:

$$\mathcal{M}_\ell b_\ell = x_{2m(\ell)+1}.$$

The number of smoothing steps $m(L)$ on the finest level is a free parameter and for the standard V-cycle $m(\ell) = m(L)$ whereas in the case of variable V-cycle this becomes $m(\ell) = m(L)2^{L-\ell}$. The smoothers \mathcal{B}_ℓ are overlapping Schwarz smoothers discussed in section (4.5). We refer to \mathcal{M}_L as the V-cycle preconditioner of \mathcal{A} . The iteration

$$x_{k+1} = x_k + \mathcal{M}_L(b_L - \mathcal{A}_L x_k) \tag{4.7}$$

is the V-cycle iteration.

4.7 Numerical Results

We test the Multigrid preconditioner with the overlapping Schwarz smoothers for the incompressible fluid flow problems. We consider the analytical solutions given in 3.30 and 3.31 as reference solution for our numerical tests. We compute errors based on these reference solutions.

4.7.1 Poiseuille Flow

We consider the domain $\Omega = [-1, 1]^2$ with inhomogeneous Dirichlet boundary conditions where the velocities at boundary of domain are give by (3.30). By choosing $\beta = u$ and $\gamma = 0$ the functions given in (3.30) solve the equation (4.1).

In Table 4.1 the convergence rates for errors are presented. We use a finite element spaces pair $RT_1 \times Q1$ and viscosity parameter $\nu = 10^{-2}$. We observe quadratic convergence in L^2 errors and linear in H^1 for both velocity and pressure, in Table 4.1.

Levels	$\ u - u_h\ _{L^2}$		$\ u - u_h\ _{H^1}$		$\ p - p_h\ _{L^2}$		$\ p - p_h\ _{H^1}$	
3	3.8515e-02	-	5.8002e-01	-	4.6650e-03	-	1.5503e-02	-
4	9.7420e-03	1.98	2.8928e-01	1.00	1.3147e-03	1.83	6.2433e-03	1.31
5	2.4967e-03	1.96	1.4449e-01	1.00	3.7782e-04	1.80	2.6985e-03	1.21
6	6.4058e-04	1.96	7.2216e-02	1.00	1.0326e-04	1.87	1.2541e-03	1.11
7	1.6318e-04	1.97	3.6098e-02	1.00	2.7518e-05	1.91	6.1207e-04	1.03
8	4.1264e-05	1.98	1.8046e-02	1.00	7.2233e-06	1.93	3.0396e-04	1.01

Table 4.1: Convergence rates for L^2 and H^1 errors of velocity and pressure

4.7.2 Kovaszny Flow

We consider the domain in this case $\Omega = [-\frac{1}{2}, \frac{3}{2}] \times [0, 2]$ where on the boundary of domain we have inhomogeneous Dirichlet boundary conditions in which the velocities are given by (3.31). The analytical solution given in (??) satisfies (4.1). In Figure 4.1 we present the velocity profile for Reynolds number 10 and 100.

The analytical solution in (3.31) is smooth for any Reynolds number which allows us to test our method for the higher order elements and any Reynolds number. In Table 4.2, we present the convergence rates of errors for velocity and pressure. We observe the optimal convergence rates of L^2 and H^1 errors of velocity and pressure. These results are obtained to reduce the residual to 10^{-10} for Reynolds number $Re = 10$.

k	ℓ	$\ u - u_h\ _{L^2}$		$\ u - u_h\ _{H^1}$		$\ p - p_h\ _{L^2}$		$\ p - p_h\ _{H^1}$	
1	5	5.6000e-02	1.88	2.6585e+00	1.00	1.1640e-01	1.76	5.6070e+00	0.90
	6	1.4541e-02	1.95	1.3270e+00	1.00	3.3487e-02	1.80	2.8676e+00	0.97
	7	3.7279e-03	1.96	6.6286e-01	1.00	9.4132e-03	1.83	1.4424e+00	0.99
2	5	3.6596e-03	2.99	2.7714e-01	1.99	1.0209e-02	2.60	7.1736e-01	1.73
	6	4.5875e-04	3.00	6.8776e-02	2.01	1.6827e-03	2.60	2.1249e-01	1.76
	7	5.7358e-05	3.00	1.7120e-02	2.01	2.8395e-04	2.57	6.5361e-02	1.70
3	5	2.0577e-04	3.84	1.8446e-02	3.01	6.6551e-04	3.50	6.5624e-02	2.66
	6	1.3806e-05	3.90	2.2682e-03	3.02	6.8288e-05	3.28	1.0231e-02	2.68
	7	8.8572e-07	3.95	2.8037e-04	3.02	4.8829e-06	3.54	1.6580e-03	2.63

Table 4.2: Convergence rates for L^2 and H^1 errors of velocity and pressure

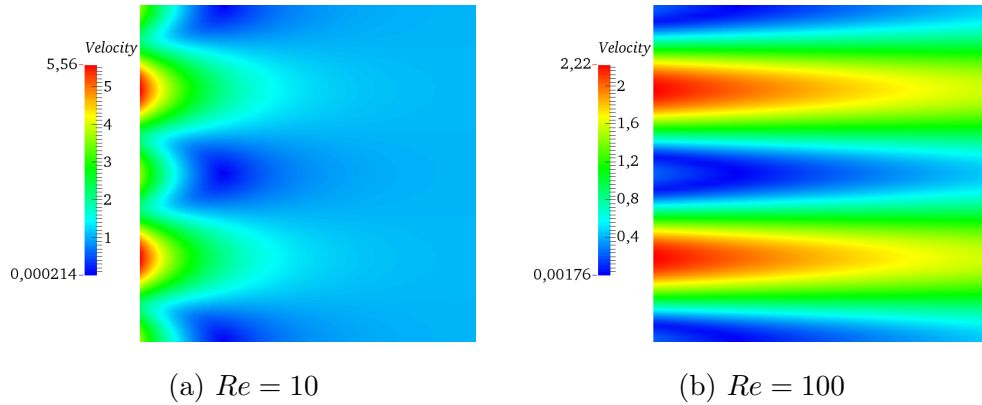


Figure 4.1: Velocity magnitude for Kovasznay flow

4.7.3 Multigrid Performance

We compute the solutions of the flow problems in our test cases with multigrid preconditioner using the multiplicative Schwarz smoothers. We describe our problem setup and parameters in following remarks.

Remark 4.7.1. *We consider the domain $\Omega = [-1, 1] \times [-1, 1]$ for all of our tests. We use DG formulation with penalty parameter dependent on each level as $\sigma_\ell = \frac{k(k+1)}{2h_\ell}$ and finite element pair $RT_1 \times Q_1$.*

Remark 4.7.2. *In all of our following numerical experiments we use Picard iteration as outer solver for non-linearity and GMRES as inner solver for linear system. We present the iterations count for Picard iteration to reduce the residual by factor of 10^6 and average iterations in each Picard iteration for inner solver to reduce the residual by a factor of 10^2 .*

	<i>ReynoldsNumbers</i>			
levels	10	100	500	1000
2	3	5	5	8
3	4	7	8	9
4	5	7	9	8
5	4	6	7	100
6	4	6	8	–
7	4	5	100	–

	<i>ReynoldsNumbers</i>			
levels	10	100	500	1000
2	1	1	1	5
3	1	3	4	18
4	3	7	13	54
5	4	17	41	100
6	5	26	100	–
7	7	31	100	–

(a) Picard iterations without sorting

(b) GMRES iterations without sorting

	<i>ReynoldsNumbers</i>			
levels	10	100	500	1000
2	3	5	5	6
3	4	7	8	8
4	4	7	8	9
5	4	6	8	8
6	4	6	8	8
7	4	6	7	8

	<i>ReynoldsNumbers</i>			
levels	10	100	500	1000
2	1	1	1	1
3	1	1	1	1
4	1	3	5	6
5	3	7	14	18
6	4	19	33	43
7	4	27	60	84

(c) Picard iterations with sorting

(d) GMRES iterations with sorting

Table 4.3: Comparison of vertex patches sorting with no sorting

4.7.3.1 Pousseuille Flow

As in case of the Oseen equations , we also have both the diffusion and convection terms in (4.1), so that we have the cases of diffusion dominated and convection dominated flow. We observe that for multiplicative Schwarz

	<i>ReynoldsNumbers</i>						
levels	1.0	10.0	50.0	100.0	500.0	1000.0	5000.0
2	5	3	6	5	5	6	6
3	3	4	6	7	8	8	8
4	3	5	6	7	8	9	10
5	3	4	5	6	8	8	10
6	3	4	5	6	8	8	9
7	3	4	5	6	7	8	15

(a) Picard iteration count

	<i>ReynoldsNumbers</i>						
levels	1.0	10.0	50.0	100.0	500.0	1000.0	5000.0
2	1	1	1	1	1	1	1
3	2	2	3	3	5	7	8
4	2	5	6	7	11	14	21
5	3	7	8	17	26	32	50
6	3	8	21	29	54	68	100
7	3	8	25	41	93	100	100

(b) GMRES iteration count

Table 4.4: Sorting in one direction, $m(\ell) = 1$.

smoothers, sorting of the vertex patches in direction of flow improves the result as presented in Table 4.3. As shown in Table 4.3 sorting is effective in case of convection dominated problems i.e. high Reynolds numbers for our linear solver, we can see this by comparison of Table 4.3b and Table 4.3d.

	<i>ReynoldsNumbers</i>						
levels	1.0	10.0	50.0	100.0	500.0	1000.0	5000.0
2	5	3	6	5	5	6	6
3	3	4	6	7	8	8	8
4	3	4	6	7	8	9	10
5	3	4	5	6	8	8	10
6	3	4	6	6	8	8	9
7	3	4	5	6	7	8	79

(a) Picard iteration count

	<i>ReynoldsNumbers</i>						
levels	1.0	10.0	50.0	100.0	500.0	1000.0	5000.0
2	1	1	1	1	1	1	1
3	1	1	1	1	1	1	1
4	1	1	2	3	5	6	8
5	1	3	7	7	14	18	29
6	1	4	13	19	33	43	79
7	2	4	16	27	60	84	100

(b) GMRES iteration count

Table 4.5: Full sweep, $m(\ell) = 1$.

For the Picard iteration, the iteration count is almost same for low Reynolds numbers. However, it simply fails in case of high Reynolds as shown in Table 4.3a. Therefore sorting in the direction of flow is necessary for solving convection dominated problems.

	<i>ReynoldsNumbers</i>						
levels	1.0	10.0	50.0	100.0	500.0	1000.0	5000
2	5	3	6	5	5	6	6
3	3	4	6	7	8	8	8
4	3	4	6	7	8	9	10
5	3	4	6	6	7	8	10
6	3	4	6	6	8	8	10
7	3	4	5	6	7	8	–

(a) Picard iteration count

	<i>ReynoldsNumbers</i>						
levels	1.0	10.0	50.0	100.0	500.0	1000.0	5000
2	1	1	1	1	1	1	1
3	1	1	1	1	1	1	1
4	1	1	2	2	3	3	5
5	1	2	5	6	10	12	18
6	1	4	12	15	28	36	58
7	1	4	15	25	59	85	–

(b) GMRES iteration count

Table 4.6: Full sweep, $m(\ell) = 2$.

In Table 4.4a, we present the iteration count for a variety of Reynolds number. From these numbers, we observe that the Picard iteration scheme is stable with respect to the mesh levels and also Reynolds numbers. Whereas, on the other hand in Table ??, we see a strong dependence of the iteration numbers

	<i>ReynoldsNumbers</i>						
levels	1.0	10.0	50.0	100.0	500.0	1000.0	5000.0
2	5	3	6	5	5	6	6
3	4	4	6	7	8	8	8
4	3	5	6	7	8	9	10
5	3	4	5	6	8	8	10
6	3	4	6	6	8	8	9
7	3	4	5	6	7	8	12

(a) Picard iteration count

	<i>ReynoldsNumbers</i>						
levels	1.0	10.0	50.0	100.0	500.0	1000.0	5000.0
2	1	1	1	1	1	1	1
3	1	1	1	1	2	3	3
4	1	2	3	5	7	9	14
5	2	4	8	10	17	22	36
6	2	5	15	22	37	46	83
7	2	4	17	28	67	86	100

(b) GMRES iteration count

Table 4.7: Sweep in 2 directions, $m(\ell) = 1$.

of GMRES, needed in each Picard iteration, on mesh levels and as well as on Reynolds numbers.

Remark 4.7.3. *From numerical results presented in 4.3, we observed that sorting of vertex patches in flow direction is necessary for robustness of multi-*

	<i>ReynoldsNumbers</i>						
levels	1.0	10.0	50.0	100.0	500.0	1000.0	5000.0
2	5	3	6	5	5	6	6
3	3	4	6	7	8	8	8
4	3	5	6	7	8	9	10
5	3	4	5	6	8	8	10
6	3	4	6	6	7	8	9
7	3	4	5	6	7	8	28

(a) Picard iteration count

	<i>ReynoldsNumbers</i>						
levels	1.0	10.0	50.0	100.0	500.0	1000.0	5000.0
2	1	1	1	1	1	1	1
3	1	1	1	1	1	1	2
4	1	2	2	3	5	5	8
5	1	3	7	7	13	17	27
6	1	4	13	19	30	41	74
7	2	4	16	27	59	77	100

(b) GMRES iteration count

Table 4.8: Sweep in 2 directions, $m(\ell) = 2$.

grid preconditioners employing multiplicative Schwarz smoothers. In all of our numerical test, for other flow problems, we will use sorting scheme.

In case of Navier-Stokes equations, our numerical results show the dependence of multigrid preconditioner on mesh parameters. We perform extensive

numerical tests to get a set of optimal parameters for multigrid method. In Table 4.4b and Table 4.5b, we show a comparison of GMRES iterations for sorting in one direction and full sweep, respectively. From this comparison, we observe that full sweep improves the results in terms of iterations reduction for linear solver. For further reduction of the linear solver iterations, we test with two smooting steps at each level ($m(\ell) = 2$). These results are presented in Table 4.6 which represents that the reduction in iterations of linear solver is not reasonable as compare to its computational cost. Similarly, for a fair tradeoff of iterations reduction and computational cost, we perform more numerical tests with a half sweep i.e. sorting in two directions. These results are presented in Table 4.7 and 4.8 for one and two smoothing steps at each level, respectively. From all of our numerical experiments, we get a set of optimal parameters, which is not computationally expensive and gives reasonable results, described in following remark.

Remark 4.7.4. *For multigrid preconditioner, we use a half sweep (sorting of vertex in two direction) and one smoothing step at each level. We use the same setting for our other flow problems.*

4.7.3.2 Cavity driven flow

In Section 4.7.3.1, we have performed extensive numerical experiments to find the best choice for multigrid parameters. Here, we present some further results for classical case of cavity driven flow by using the same parameters for multigrid as described in Remark 4.7.4. In Table 4.9a we show the iteration count of Picard iteration scheme for various Reynolds number and we present the iteration count for GMRES in Table 4.9b. We observe the dependence of

	<i>ReynoldsNumbers</i>					
levels	1.0	10.0	50.0	100.0	500.0	1000.0
3	3	5	8	11	22	19
4	3	4	7	9	29	38
5	2	3	6	7	22	27
6	2	3	5	6	16	17
7	2	3	4	5	10	14
8	3	2	3	4	9	13

(a) Picard iterations

	<i>ReynoldsNumbers</i>					
levels	1.0	10.0	50.0	100.0	500.0	1000.0
3	1	1	1	1	1	1
4	1	1	1	1	1	1
5	1	1	1	1	1	2
6	1	1	1	1	1	3
7	1	1	1	2	5	9
8	4	1	1	2	17	18

(b) GMRES iterations

Table 4.9: Cavity driven flow

multigrid preconditioners on both mesh parameters and Reynolds numbers for this case, as we have observed in Section 4.7.3.1. However, we observe the robustness and mesh independence of our solver in case of low Reynolds number.

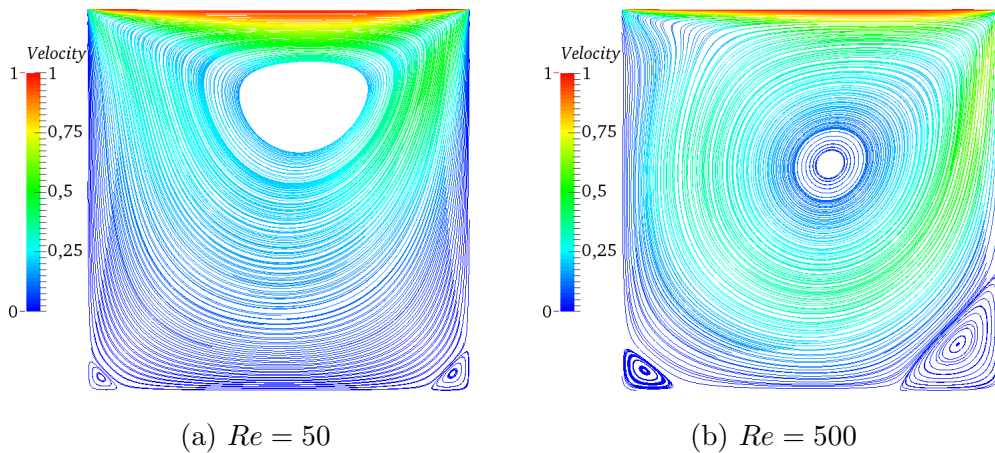


Figure 4.2: Velocity magnitude for Cavity driven flow

In Fig. 4.2 we present the numerical solution of the cavity driven flow for different Reynolds numbers. We observe three vortices for Reynolds number 500 which is the classical case for Reynolds number greater than 400.

4.7.3.3 Flow behind an obstacle (diamond)

In this section, we present the numerical results for a different flow problem. We consider the problem of flow behind an obstacle. We apply the multi-grid preconditioners with multiplicative Schwarz smoothers for solving the system of linear equations arising from the discretization of Navier-Stokes equations. For this model problem, we use the geometry as shown in Fig. 4.3 with $H = 4.1$. We use inhomogeneous boundary conditions given in 3.30. This is classical test case, usually used for time dependent problems. However, we only present numerical results for stationary case.

We use the same parameters for multigrid as described in Remark 4.7.4. In this problem our coarse mesh contains 60 cells, whereas in previous examples



Figure 4.3: Geometry of Problem

	<i>ReynoldsNumbers</i>				
levels	1	10	50	100	200
2	4	7	4	7	20
3	4	7	4	6	19
4	4	6	4	5	20
5	4	4	7	16	31

(a) Picard iterations

	<i>ReynoldsNumbers</i>				
levels	1	10	50	100	200
2	1	1	1	1	4
3	1	1	1	4	13
4	1	4	1	3	30
5	1	2	1	3	8

(b) GMRES iterations

Table 4.10: Flow behind an obstacle

the coarse mesh was 1 cell only. Hence, our tests are only upto 5 levels in multigrid setting. In Table 4.10, we present the results for our solver where Table 4.10a represents the number of Picard iterations to reduce the residual to 10^{-6} and Table 4.10b represents the number of GMRES iterations. The results in Table 4.10 are for low Reynolds numbers on different refinement

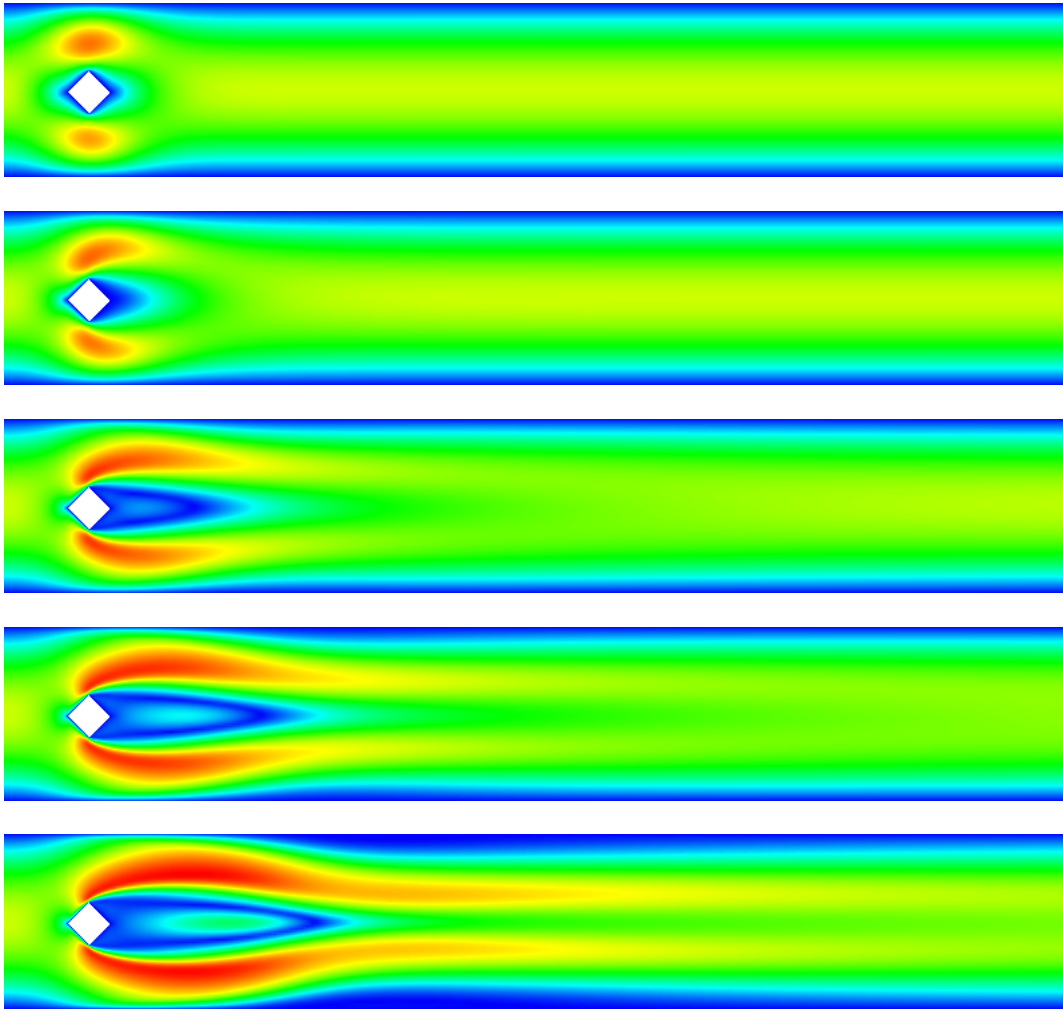


Figure 4.4: Velocity magnitude for flow behind an obstacle, top to bottom $Re = 1, 10, 50, 100, 200$.

levels. We observe the robustness of our solver from numerical results. However, we also observe dependence of multigrid solver on mesh parameters and Reynolds number.

In Fig. 4.4 we present the velocity profile for our numerical solution for dif-

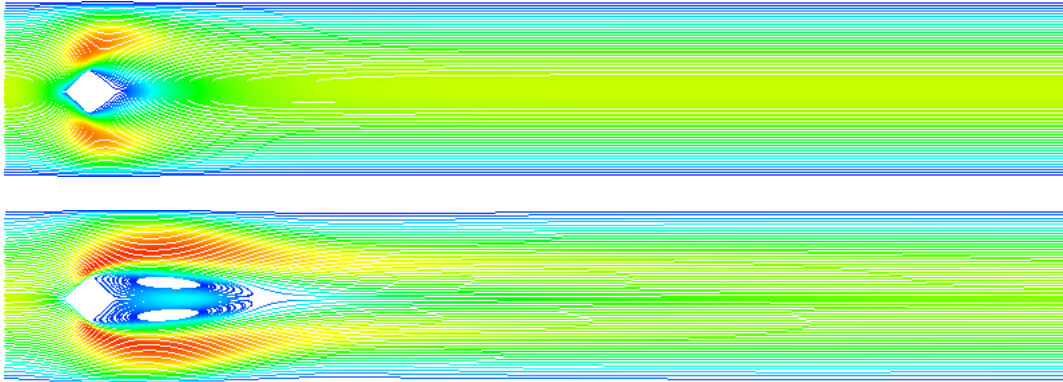


Figure 4.5: Streamlines for velocity profiles for Obstacle Problem $Re = 10$ (top) and $Re = 100$ (bottom)

ferent Reynolds numbers. This type of flow problem is a classical test for Navier-Stokes solvers. We know from literature, the regime where vortices start developing, which is value of Reynolds number around 90. We show this fact in Fig. 4.5, where we present the streamlines for velocity profile for Reynolds number 10 and 100. In case of Reynolds number 100 we observe the vortices developing behind the obstacle, where as in case of Reynolds number 10 there are no vortices.

4.8 Summary

In this chapter, we presented extensive numerical results for Navier-Stokes equations using multigrid preconditioners with overlapping multiplicative Schwarz smoothers. In case of Navier-Stokes equations, we have two difficulties: non-linearity and non-symmetry. For solving non-linearity, we used Picard iteration scheme as outer solver. We used GMRES as inner solver pre-

conditioned with multigrid preconditioner, to solve the linear system in each Picard iteration. We applied the theory of symmetric problems for building our multigrid preconditioners. In view of our numerical results, we have seen the dependence of our multigrid preconditioners on mesh parameters and the Reynolds number. However, our solver is robust for low Reynolds numbers.

Chapter 5

The Brinkman Equations

5.1 Introduction

In this chapter, we present the multigrid preconditioner for the finite element approximations of flow problems in highly heterogeneous porous media governed by the Brinkman systems. For solving the Brinkman problem numerically, there exist various approaches in the literature for approximation of the Brinkman problem using modifications of stable elements for Stokes and Darcy equations. Examples include, modifications based on Stokes elements with various stabilization techniques (e.g., [4, 18, 25, 39, 40, 56]), modifications based on Darcy elements (e.g. [56, 60, 78]), the coupling of Stokes and Darcy flows (e.g. [20, 53, 58, 61]) and elements directly constructed for Brinkmans equations (cf. [19, 80]). However, we use the H^{div} -conforming discontinuous Galerkin method [24, 22, 76] for the discretization of Brinkman equations to account for the incompressibility constraint on discrete level.

For resolving the fine scale structures in heterogeneous media, we end up with very large algebraic systems. Further difficulty arises due to the high variations in the permeability resulting ill-conditioned algebraic systems. There are some approaches in existing literature, to tackle these problems, mainly Multiscale methods (e.g. [13, 38, 47, 29, 28, 6, 5, 3, 45, 77]) and Algebraic Multigrid methods (e.g. [27, 26, 73, 74]).

For large ill-conditioned algebraic system, arising from the discretization of Brinkman equations, geometric multigrid methods have recently proven to be efficient by Kanschat and Mao [51]. In their work they have considered Brinkman equations without inertial term, whereas in this chapter we extend the idea of applying multigrid preconditioners to the nonlinear Brinkman equations. We provide the numerical results for the Brinkman equations in both cases, namely, the linear Brinkman equations and the nonlinear Brinkman equations (including convection term). Although, we lack the theory for non-symmetric problems, however, we observe from our computational results that the multigrid method is robust with respect to the mesh size and the permeability contrast for highly heterogeneous media.

5.2 Linear Brinkman

5.2.1 Model Problem

Flow in porous media is modelled by Darcy law as

$$u = -\frac{\tilde{\kappa}}{\mu} \nabla p. \quad (5.1)$$

However, in the cases of flow through heterogeneous media with large pores, the Darcy's law alone is not sufficient for modeling these flow problems. In large pores flow is governed by Stokes law. Hence, we consider the Brinkman model [17] for the macroscopic pressure p and the fluid velocity u :

$$\begin{aligned} -\mu\Delta u + \kappa u + \nabla p &= f && \text{in } \Omega, \\ \nabla \cdot u &= 0 && \text{in } \Omega, \\ u &= g && \text{on } \partial\Omega, \end{aligned} \tag{5.2}$$

where $f \in L^2(\Omega)^d$ is a prescribed external body force, μ is the viscosity coefficient which can be different from the fluid viscosity in general but we use the same coefficient. We get the Darcy model in the limiting case of $\mu = 0$. Here κ is inverse permeability coefficient depending on the space variables and bounded as following with the assumption that κ_{min} and κ_{max} are positive constants.

$$0 < \kappa_{min} < \kappa < \kappa_{max} < \infty \quad \forall x \in \Omega, \tag{5.3}$$

We are using the same notation κ for inverse permeability coefficient as it is used in Darcy's law (5.1) for permeability coefficient, which means that $\kappa = \frac{\mu}{\bar{\kappa}}$.

5.2.2 Discontinuous Galerkin discretization

We use the discontinuous Galerkin discretizations for diffusion term and incompressibility condition in (5.2). For diffusion term, we use the interior penalty method of [9]. By using the notations mention in section 2.3 for jumps and averages, the interior penalty bilinear form for the diffusion term

including the reaction term can be written as

$$\begin{aligned}
a_\ell(u, v) &= \mu (\nabla u, \nabla v)_{\mathcal{T}_\ell} + (\kappa u, v)_{\mathcal{T}_\ell} + 2\mu\sigma_L \langle \llbracket u \rrbracket, \llbracket v \rrbracket \rangle_{\mathcal{F}_\ell^i} \\
&\quad - \mu \langle \{\!\{ \nabla u \}\!\} \cdot \mathbf{n}, \llbracket v \rrbracket \rangle_{\mathcal{F}_\ell^i} - \mu \langle \{\!\{ \nabla v \}\!\} \cdot \mathbf{n}, \llbracket u \rrbracket \rangle_{\mathcal{F}_\ell^i} \\
&\quad + 2\mu\sigma_L \langle u, v \rangle_{\mathcal{F}_\ell^\partial} - \mu \langle \partial_n u, v \rangle_{\mathcal{F}_\ell^\partial} - \mu \langle \partial_n v, u \rangle_{\mathcal{F}_\ell^\partial},
\end{aligned}$$

where $\{\!\{ \nabla v \}\!\}$ is the average of the $d \times d$ matrix ∇v . The parameter σ_L is interior penalty parameter chosen sufficiently large in such a way that it ensures the coercivity of the form $a_\ell(\cdot, \cdot)$. We can estimate its lower limit for a boundary face $F \in \mathcal{F}$ of a cell T by

$$\sigma_L > \frac{k(k+1)}{2h_L},$$

where k is the degree of the polynomial of shape functions and h_L is the mesh size finest level L . We usually choose twice the value in our numerical test. The discrete weak formulation of (5.2) reads now: find $(u_\ell, p_\ell) \in V_\ell \times Q_\ell$ such that for all test functions $v_\ell \in V_\ell$ and $q_\ell \in Q_\ell$ there holds

$$\begin{aligned}
\mathcal{A}_\ell \left(\begin{pmatrix} u_\ell \\ p_\ell \end{pmatrix}, \begin{pmatrix} v_\ell \\ q_\ell \end{pmatrix} \right) &\equiv a_\ell(u_\ell, v_\ell) + (p_\ell, \nabla \cdot v_\ell) - (q_\ell, \nabla \cdot u_\ell) \\
&= \mathcal{F}(v_\ell, q_\ell) \equiv (f, v_\ell) \quad \forall v_\ell \in V_\ell, q_\ell \in Q_\ell. \quad (5.4)
\end{aligned}$$

5.2.3 Existence and Uniqueness of Solution

We are using the spaces RT_k/Q_k for which the pair of local spaces V_T/Q_T satisfy the divergence free condition. Thus for pair of Raviart-Thomas spaces we have

$$\nabla \cdot RT_k = Q_k.$$

The resulting space V_ℓ is equipped with the norm.

$$\|u\|_\sigma^2 = \sum_{T \in \mathcal{T}_\ell} \|\nabla u\|_{L^2(T)}^2 + \sum_{F \in \mathcal{F}_\ell} \int_F \sigma_L |\{u \otimes \mathbf{n}\}|^2 ds + \|u\|_{\kappa, L^2(\Omega)}^2,$$

where $\|u\|_{\kappa, L^2(\Omega)}^2 = \int_\Omega \kappa u \cdot u dx$. For the existence and uniqueness of solution we need continuity and coercivity of the form $\mathcal{A}_\ell(\cdot, \cdot)$ for which we have the following estimates for the Laplacian, convection term and incompressibility constraint. For the proofs of the proposition we refer to [21, 22]

Proposition 5.2.1. *If the interior penalty parameter is chosen sufficiently large, then there exist constants $c_a >$ and $\alpha > 0$, independent of multigrid mesh level ℓ , such that*

$$\begin{aligned} a_\ell(u, v) &\leq c_a \|u\|_\sigma \|v\|_\sigma, & u, v \in V_\ell \\ a_\ell(u, u) &\geq \alpha \|u\|_\sigma^2, & u \in V_\ell \end{aligned}$$

Proof. Proof is given in [59]. □

Proposition 5.2.2. *For any pressure function $q \in Q_\ell$, there exists a velocity function $v \in V_\ell$, satisfying*

$$\inf_{q \in Q_\ell} \sup_{v \in V_\ell} \frac{(q, \nabla \cdot v)}{\|v\|_\sigma \|q\|_{L^2(\Omega)}} \geq \gamma_\ell > 0 \quad (5.5)$$

where $\gamma_\ell = c \sqrt{\frac{h_L}{h_\ell}} = c \sqrt{2^{L-\ell}}$ and c is a constant independent of the multigrid level ℓ .

Proof. From the relation (5.3), we have bounds for κ . By using the constants in (5.3), the κ -dependent norm can be bounded. Then Proposition 3.4.3 leads to 5.5. The complete proof is given in [59]. □

5.2.4 Overlapping Schwarz Smoothers

In this section we present overlapping Schwarz smoother of multiplicative type used for the multigrid preconditioners. We have done a detailed discussion on these type of smoothers, in Section 3.6. Here, we use the same smoothers for Brinkman problem. We define multiplicative Schwarz smoothers by using the following projection like operator

$$\mathcal{A}_{\ell,\nu} \left(\mathcal{P}_{\ell,\nu} \begin{pmatrix} u_\ell \\ p_\ell \end{pmatrix}, \begin{pmatrix} v_{\ell,\nu} \\ q_{\ell,\nu} \end{pmatrix} \right) = \mathcal{A}_\ell \left(\begin{pmatrix} u_\ell \\ p_\ell \end{pmatrix}, \begin{pmatrix} v_{\ell,\nu} \\ q_{\ell,\nu} \end{pmatrix} \right) \quad \forall \begin{pmatrix} v_{\ell,\nu} \\ q_{\ell,\nu} \end{pmatrix} \in X_{\ell,\nu} \quad (5.6)$$

where $X_{\ell,\nu} = V_{\ell,\nu} \times Q_{\ell,\nu}$. The symmetric multiplicative Schwarz smoother \mathcal{B}_ℓ using the error propagation operators, associated with spaces $X_{\ell,\nu}$, are

$$\mathcal{B}_\ell = (\mathcal{I} - \mathcal{E}_\ell^* \mathcal{E}_\ell) \mathcal{A}_\ell^{-1} \quad \text{with} \quad \mathcal{E}_\ell = (\mathcal{I} - \mathcal{P}_{\ell,1}) \cdots (\mathcal{I} - \mathcal{P}_{\ell,N_\ell}) \quad (5.7)$$

where \mathcal{E}_ℓ^* is the \mathcal{A}_ℓ -adjoint of \mathcal{E}_ℓ .

We give an overview of smoothers for Brinkman problem without the convergence analysis which can be found in [59], for symmetric problems. In this section, we apply this theory for numerical results for the Brinkman equations. Afterwards, in Section 5.3, we want to extend this approach to non-symmetric problems and there is very little work done on theoretical aspects of non-symmetric problems. Hence, we take advantage from theory of symmetric problems and apply the same approach to obtain numerical results presented in later sections.

5.2.5 Multigrid preconditioner

We adapt the same approach for building our multigrid preconditioner as described in section 3.7. The multigrid preconditioner $\mathcal{M}_\ell : X_\ell \longrightarrow X_\ell$

where $(X_\ell = V_\ell \times Q_\ell)$ is defined recursively in V-cycle with $m(\ell) \geq 1$ pre and post smoothing steps. Let \mathcal{B}_ℓ be suitable smoother. We assume that the coarse mesh problem $\mathcal{A}_0 x_0 = b_0$ has a small size so that we directly invert \mathcal{A}_0 and have $\mathcal{M}_0 = \mathcal{A}_0^{-1}$. For $\ell \geq 1$, we define the action of \mathcal{M}_ℓ on a vector $b_\ell \in X_\ell$ as follows:

- Pre-smoothing:

$$x_i = x_{i-1} + \mathcal{B}_\ell(b_\ell - \mathcal{A}_\ell x_{i-1}) \quad i = 1, \dots, m(\ell).$$

- Coarse grid correction:

$$x_{m(\ell)+1} = x_{m(\ell)} + \mathcal{I}_{\ell-1}^T \mathcal{M}_{\ell-1} \mathcal{I}_{\ell-1}(b_\ell - \mathcal{A}_\ell x_{m(\ell)}),$$

where \mathcal{I}_ℓ^T and \mathcal{I}_ℓ are the same operators as defined in section 3.7.1.

- Post-smoothing:

$$x_i = x_{i-1} + \mathcal{B}_\ell(b_\ell - \mathcal{A}_\ell x_{i-1}) \quad i = m(\ell) + 2, \dots, 2m(\ell) + 1.$$

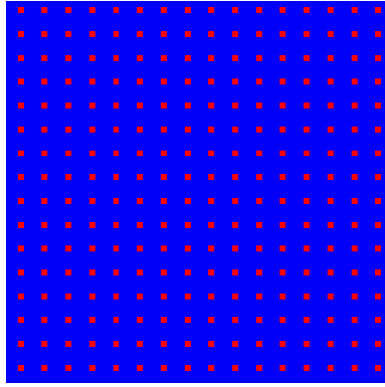
- Assign:

$$\mathcal{M}_\ell b_\ell = x_{2m(\ell)+1}.$$

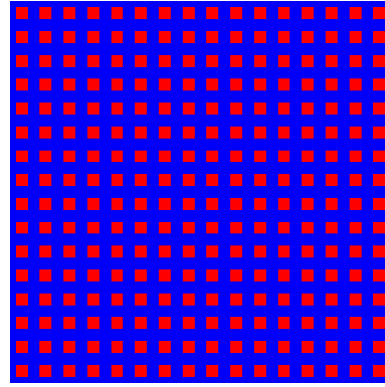
The number $m(L)$ of smoothing steps on the finest level is a free parameter. For the standard V-cycle, $m(\ell) = m(L)$. In the case of variable V-cycle, this becomes $m(\ell) = m(L)2^{L-\ell}$. The smoothers \mathcal{B}_ℓ are overlapping Schwarz smoothers discussed in section (5.2.4). We refer to \mathcal{M}_L as the V-cycle preconditioner of \mathcal{A} . The iteration

$$x_{k+1} = x_k + \mathcal{M}_L(b_L - \mathcal{A}_L x_k), \quad (5.8)$$

is the V-cycle iteration.



(a) Sparse periodic geometry



(b) Dense periodic geometry

Figure 5.1: Inverse Permiability coefficient (κ) distribution

5.2.6 Numerical Results

In this section, we present the numerical results for the Brinkman model. We present test results for high contrast in permeability coefficients for two different types of distributions, see Fig. 5.1 red regions show highly permeable porous media and blue regions present lowly permeable porous media. In Fig. 5.1a, we present a periodic distribution of cells of size $1/64$ (colored red) with low permeability and rest of the region (colored blue) is highly permeable or can be considered as free fluid region with low permeable cells as obstacles. In Fig. 5.1b, we increase the size of these cells to $1/32$ to create another heterogeneous media for computational results. These periodic geometries are classical tests for solvers, used by many other researcher (e.g. [2], [46], [44], [51], [59]).

Remark 5.2.1. *In all numerical tests we consider the 2D domain $\Omega =$*

$(0, 1) \times (0, 1)$ a unit square. We use the Dirichlet boundary conditions $u = \begin{pmatrix} 1 \\ 0 \end{pmatrix}$ and $\mathbf{f} = 0$. The distribution of the inverse permeability coefficients is $\kappa = 1$ in blue regions and $\kappa = 10^4, 10^5, 10^6$ in red regions of the Sparse periodic geometry and Dense periodic geometry.

5.2.6.1 MG Performance

We have performed numerical tests using the multigrid preconditioner with overlapping Schwarz smoothers of multiplicative type. We present the performance of the multigrid preconditioners in this section for Darcy and Brinkman problems, where the problem setup is described in remark 5.2.1. We consider constant viscosity $\nu = 0.01$ for both regions in case of Brinkman problem and $\nu = 0$ in case of Darcy problem.

For multigrid preconditioner, we apply standard V-cycle algorithm with overlapping multiplicative Schwarz smoothers with one smoothing step at each level. We use the uniform mesh refinements and the penalty parameter in DG formulation as $\sigma_\ell = \frac{k(k+1)}{2h_\ell}$, where h_ℓ is the mesh size at level ℓ and k is the degree of polynomial. We use the finite element pair $RT_1 \times Q_1$ in all of our numerical tests. GMRES solver is set to reduce the residual to 10^{-6} .

Remark 5.2.2. (*Upscaling and downscaling*)

The upscaling is considered to have dominant effect in case of multi-scale methods whereas its impact is considered less dominant in preconditioning perspective. However, we have a different observation in our numerical experiments. We are building multigrid preconditioners using coarser levels where heterogeneity of media is not resolved by mesh and hence solving on finer levels where heterogeneous media is aligned with the mesh. In our re-

sults, we have used no upscaling, which means, we consider the homogeneous porous media with high permeability on coarser levels. We have observed an improvement of about 40% in iteration count as compared to the results presented in [59] and [51] with a different upscaling scheme. For the downscaling scheme, we have the same approach as presented in above mentioned works. The downscaling is done through simple inheritance.

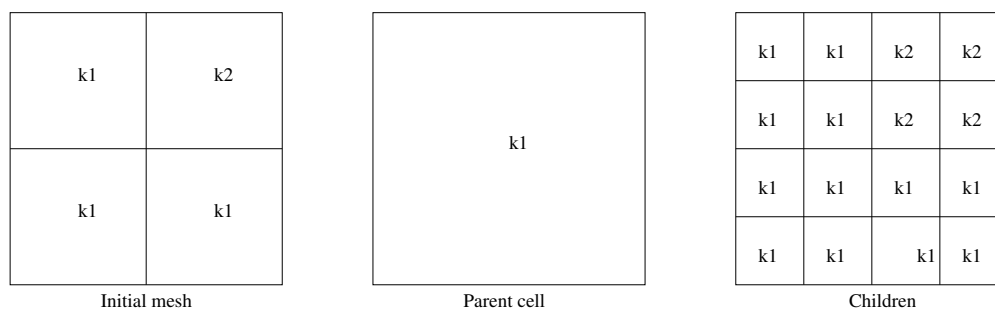


Figure 5.2: Upscaling and downscaling

level	Sparse periodic geometry			Dense periodic geometry		
	$\kappa = 10^4$	$\kappa = 10^5$	$\kappa = 10^6$	$\kappa = 10^4$	$\kappa = 10^5$	$\kappa = 10^6$
8	3	3	6	5	5	5
9	3	3	4	4	4	5
10	3	3	4	4	4	4

Table 5.1: Darcy: GMRES iteration count for different inverse permeability coefficient κ for Sparse periodic geometry

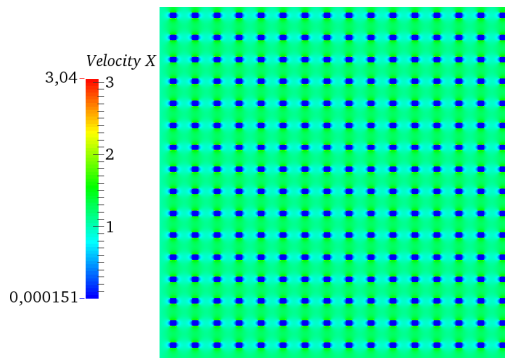
In Table 5.1, we present the iteration count of GMRES for Darcy problems using Sparse periodic geometry and Dense periodic geometry. In columns of

Table 5.1, we show different permeability contrasts and in rows multigrid levels. The coarsest level in the multi-level hierarchy, contains only one cell. In this case, our mesh size at level 8 is 1/128. We build multigrid preconditioners using upscaling and downscaling as described in remark 5.2.2. We observed that our solver is robust and is independent of the mesh parameters and variations in permeability coefficients. Furthermore, we provide the numerical solution for different permeability contrast for both geometries in Fig. 5.3 and Fig. 5.4, where we show only x-component of velocity and pressure.

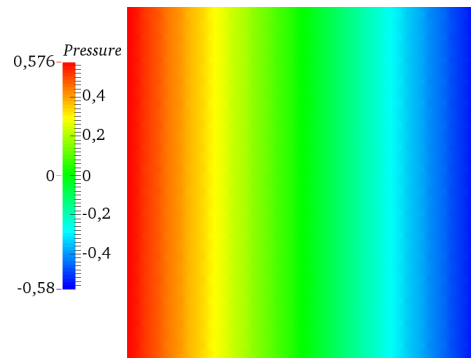
level	Sparse periodic geometry			Dense periodic geometry		
	$\kappa = 10^4$	$\kappa = 10^5$	$\kappa = 10^6$	$\kappa = 10^4$	$\kappa = 10^5$	$\kappa = 10^6$
8	8	8	7	10	10	10
9	7	6	5	9	8	7
10	6	6	11	8	7	11

Table 5.2: Brinkman: GMRES iteration count for different inverse permeability coefficient κ for Dense periodic geometry

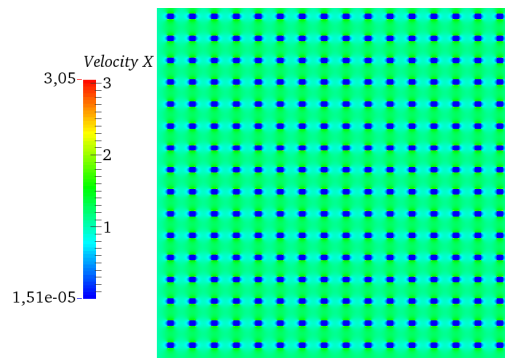
Similarly, we show the iteration count of GMRES for the Brinkman problems using the Sparse periodic geometry and Dense periodic geometry in Table 5.2. The columns of Table 5.2 represent the iteration count for different permeability contrasts and the multigrid levels are presented in rows. For multigrid preconditioner, we take the same approach as for the Darcy problems. We observed that our solver is independent of permeability contrast as can be seen in rows. Further, it is independent of the mesh as shown in



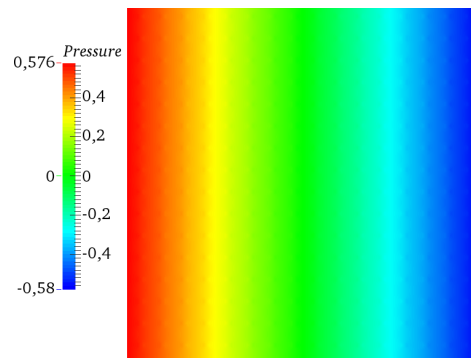
(a) Velocity x-component for $\kappa = 10^4$



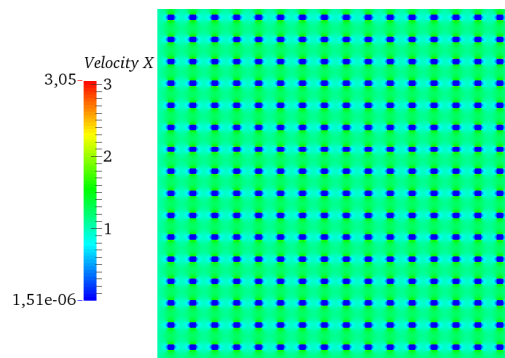
(b) Pressure for $\kappa = 10^4$



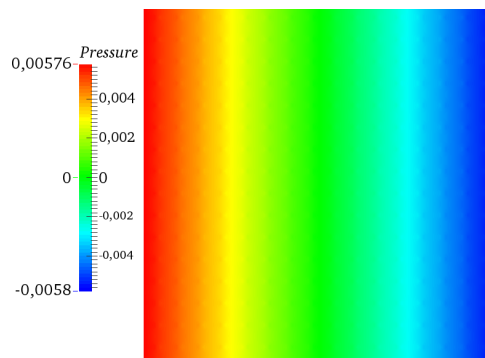
(c) Velocity x-component for $\kappa = 10^5$



(d) Pressure for $\kappa = 10^5$

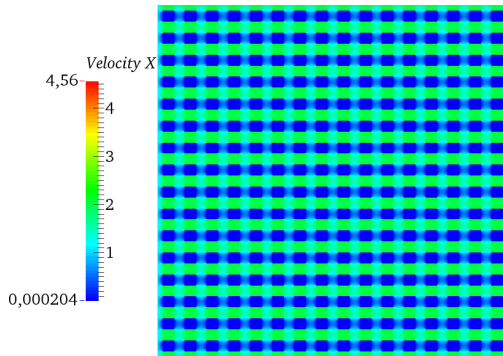


(e) Velocity x-component for $\kappa = 10^6$

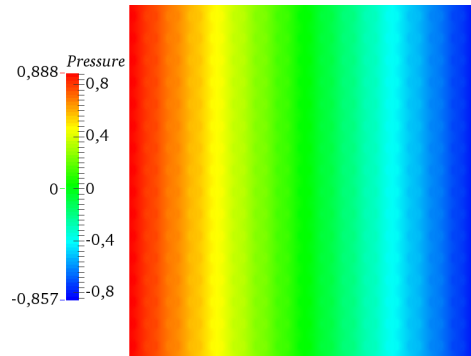


(f) Pressure for $\kappa = 10^6$

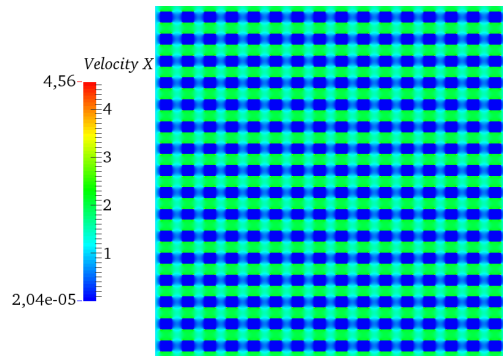
Figure 5.3: Darcy: Solution for Sparse periodic geometry



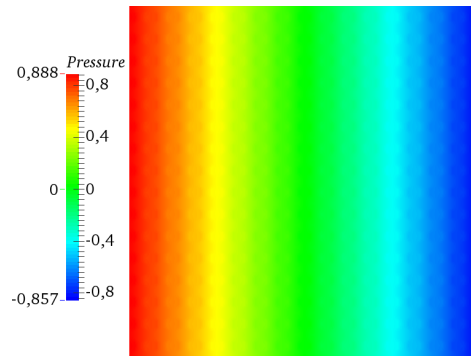
(a) Velocity x-component for $\kappa = 10^4$



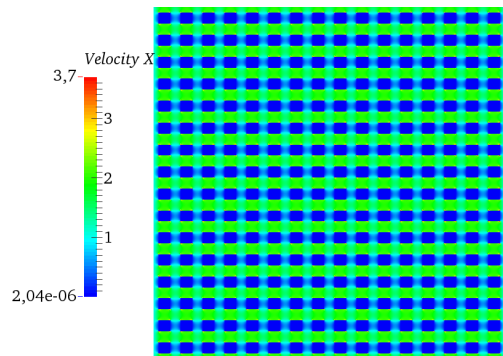
(b) Pressure for $\kappa = 10^4$



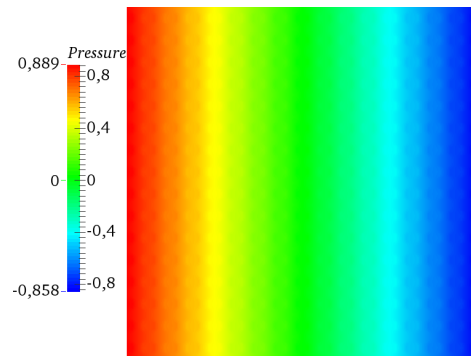
(c) Velocity x-component for $\kappa = 10^5$



(d) Pressure for $\kappa = 10^5$



(e) Velocity x-component for $\kappa = 10^6$

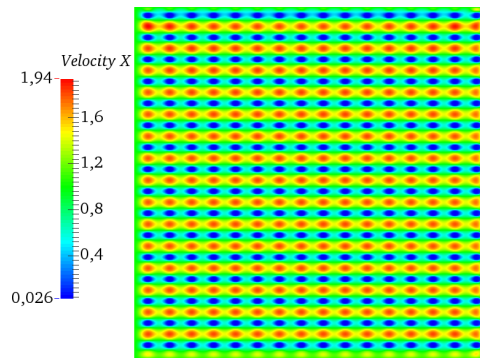


(f) Pressure for $\kappa = 10^6$

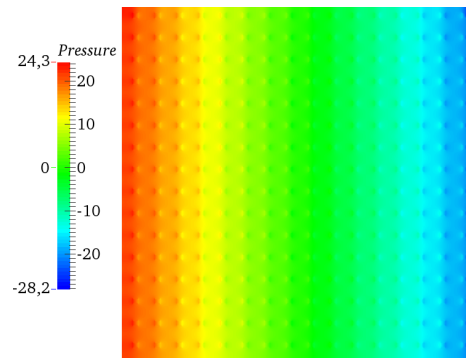
Figure 5.4: Darcy: Solution for Dense periodic geometry

columns. We present the numerical solution for the Brinkman solver for both geometries in Fig. 5.5 and Fig. 5.6, where we show only the x-component of velocity and pressure for the sake of simplicity. We can see pronounced effect of diffusion term in solutions for the Brinkman problem compared to the solutions for Darcy problem where we do not have any diffusion. Moreover, the effect of diffusion becomes less pronounced in case of decreasing permeability of obstacle cells.

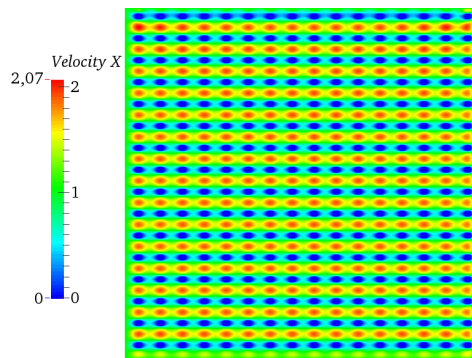
For the numerical results presented Table 5.1 and 5.2, we have used two different periodic geometries. The Dense periodic geometry is a classical test used in many works as mentioned earlier in this section. We have performed the same numerical tests as given in [51, 59], where we changed only the upscaling scheme as mentioned in remark 5.2.2. We have observed an improvement in iteration count which shows that the upscaling in preconditioning has an impact as well. However, this is only observation in numerical experiments which are limited to only periodic geometries. One can perform these numerical test with our solvers for different geometries, e.g. Vuggy media or industrial foams, as an extension for further observations of different upscaling schemes.



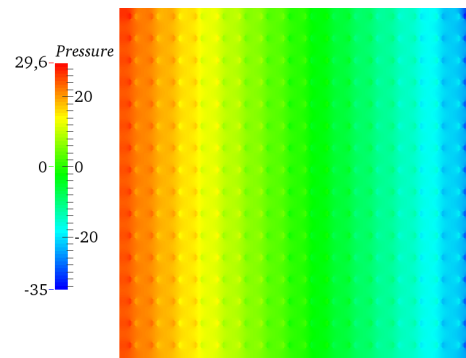
(a) Velocity x-component for $\kappa = 10^4$



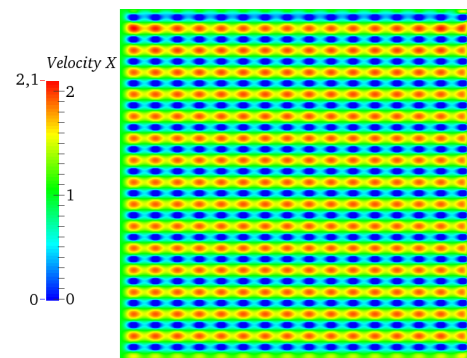
(b) Pressure for $\kappa = 10^4$



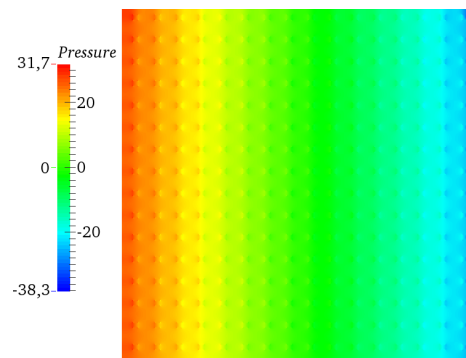
(c) Velocity x-component for $\kappa = 10^5$



(d) Pressure for $\kappa = 10^5$

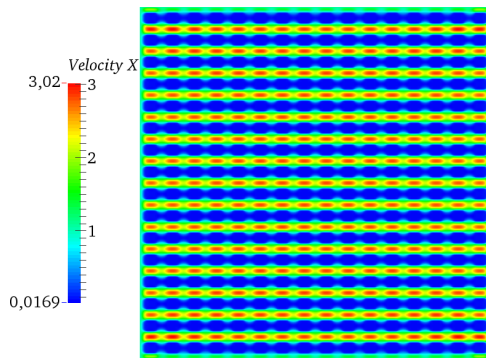


(e) Velocity x-component for $\kappa = 10^6$

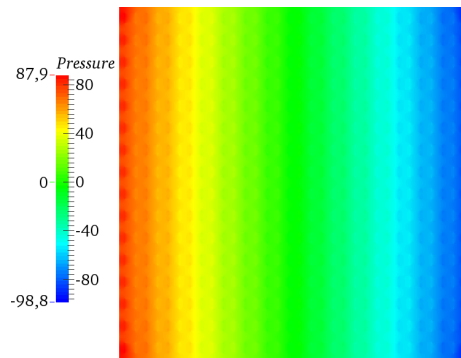


(f) Pressure for $\kappa = 10^6$

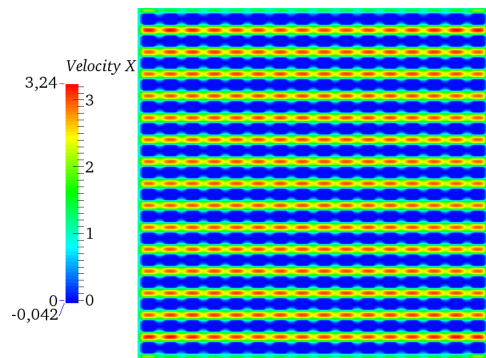
Figure 5.5: Brinkman: Solution for Sparse periodic geometry



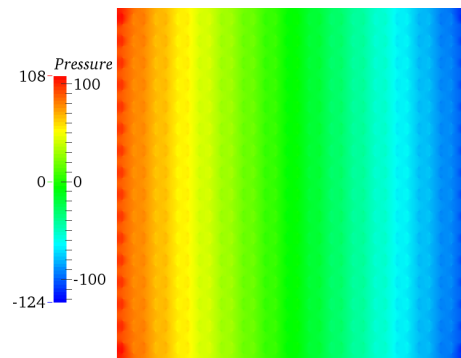
(a) Velocity x-component for $\kappa = 10^4$



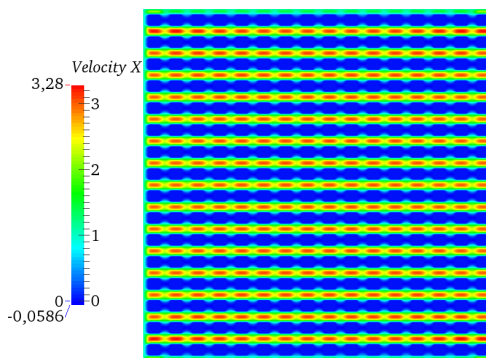
(b) Pressure for $\kappa = 10^4$



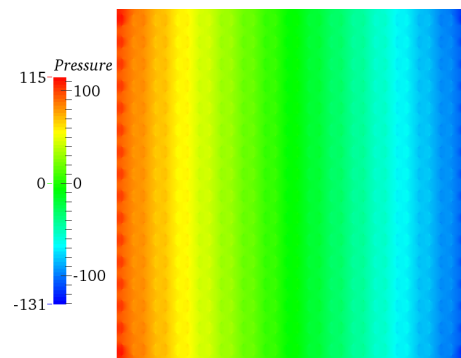
(c) Velocity x-component for $\kappa = 10^5$



(d) Pressure for $\kappa = 10^5$



(e) Velocity x-component for $\kappa = 10^6$



(f) Pressure for $\kappa = 10^6$

Figure 5.6: Brinkman: Solution for Dense periodic geometry

5.3 Nonlinear Brinkman

In this section, we discuss the Brinkman model including the convection term. We consider that for high porosity the nonlinear Brinkman model is more suitable as the fluid flow in large pores is modeled by the Navier-Stokes equations. It has been described by Brinkman [17] where the inertial term is neglected. However, there is no argument about smallness or negligibility of the inertial term. Hence, we present empirical results to show the performance of multigrid method for the nonlinear Brinkman equations.

After discretization by divergence conforming DG method, we apply multigrid preconditioners with overlapping Schwarz smoothers to solve the resulting algebraic system. We use Picard iteration for solving non-linearity. We observe from our computational results that the multigrid method is efficient and robust with respect to the mesh size and the permeability contrast for highly heterogeneous media.

We consider the Brinkman model with convective term for the macroscopic pressure p and the fluid velocity $u = (u_1, \dots, u_d)$:

$$\begin{aligned} -\mu\Delta u + (u \cdot \nabla) u + \kappa u + \nabla p &= \mathbf{f} && \text{in } \Omega, \\ \nabla \cdot u &= 0 && \text{in } \Omega, \\ u &= \mathbf{g} && \text{on } \partial\Omega, \end{aligned} \tag{5.9}$$

where $\mathbf{f} \in L^2(\Omega)^d$ is the prescribed external body force, μ is the viscosity coefficient and we get the Darcy model by setting $\mu = 0$. Here κ is permeability coefficient.

5.3.1 Discontinuous Galerkin discretization

We use discontinuous Galerkin discretization for the Brinkman equations including convective term. The discretization for the diffusion term and incompressibility is same as described in Section 5.2.2. Here, we describe the discretization for convective term using upwinding form as

$$b_\ell(\beta; u, v) = - (u, \nabla \cdot v \otimes \beta)_{\mathcal{T}_\ell} + 2 \langle |\beta \cdot \mathbf{n}| u^\uparrow, \llbracket v \rrbracket \rangle_{\mathcal{F}_\ell^i} + 2 \langle |\beta \cdot \mathbf{n}| u, v \rangle_{\mathcal{F}_\ell^p},$$

where $\beta = u$.

The discrete weak formulation of (5.2) reads now: find $(u_\ell, p_\ell) \in V_\ell \times Q_\ell$ such that for all test functions $v_\ell \in V_\ell$ and $q_\ell \in Q_\ell$ there holds

$$\begin{aligned} \mathcal{A}_\ell \left(\begin{pmatrix} u_\ell \\ p_\ell \end{pmatrix}, \begin{pmatrix} v_\ell \\ q_\ell \end{pmatrix} \right) &\equiv a_\ell(u_\ell, v_\ell) + b_\ell(\beta; u_\ell, v_\ell) + (p_\ell, \nabla \cdot v_\ell) - (q_\ell, \nabla \cdot u_\ell) \\ &= \mathcal{F}(v_\ell, q_\ell) \equiv (f, v_\ell) \quad \forall v_\ell \in V_\ell, q_\ell \in Q_\ell. \end{aligned} \quad (5.10)$$

5.3.2 Multigrid preconditioner

In the case of non-symmetric problems though we do not have sufficient theory but we apply the same method of multigrid preconditioning as it is for symmetric problems. Hence, we build our multigrid preconditioner on the same lines as described in section 5.2.5.

The multigrid preconditioner $\mathcal{M}_\ell : X_\ell \rightarrow X_\ell$ where $(X_\ell = V_\ell \times Q_\ell)$ is defined recursively in V-cycle with $m(\ell) \geq 1$ pre and post smoothing steps. Let \mathcal{B}_ℓ be suitable smoother. We assume that the coarse mesh problem $\mathcal{A}_0 x_0 = b_0$

has a small size so that we directly invert \mathcal{A}_0 and have $\mathcal{M}_0 = \mathcal{A}_0^{-1}$. For $\ell \geq 1$, we define the action of \mathcal{M}_ℓ on vector $b_\ell \in X_\ell$ as follows:

- Pre-smoothing:

$$x_i = x_{i-1} + \mathcal{B}_\ell(b_\ell - \mathcal{A}_\ell x_{i-1}) \quad i = 1, \dots, m(\ell).$$

- Coarse grid correction:

$$x_{m(\ell)+1} = x_{m(\ell)} + \mathcal{M}_{\ell-1} \mathcal{I}_{\ell-1}^t (b_\ell - \mathcal{A}_\ell x_{m(\ell)}),$$

where \mathcal{I}_ℓ^T and \mathcal{I}_ℓ are the same operators as defined in section 3.7.1.

- Post-smoothing:

$$x_i = x_{i-1} + \mathcal{B}_\ell(b_\ell - \mathcal{A}_\ell x_{i-1}) \quad i = m(\ell) + 2, \dots, 2m(\ell) + 1.$$

- Assign:

$$\mathcal{M}_\ell b_\ell = x_{2m(\ell)+1}.$$

The number $m(L)$ of smoothing steps on the finest level is a free parameter and for the standard V-cycle $m(\ell) = m(L)$ whereas in the case of variable V-cycle this becomes $m(\ell) = m(L)2^{L-\ell}$. The smoothers \mathcal{B}_ℓ are overlapping Schwarz smoothers discussed in section (5.2.4). We refer to \mathcal{M}_L as the V-cycle preconditioner of \mathcal{A} . The iteration

$$x_{k+1} = x_k + \mathcal{M}_L(b_L - \mathcal{A}_L x_k), \tag{5.11}$$

is the V-cycle iteration.

5.3.3 Numerical Results

In this section, we present the numerical results for the Brinkman model including the convection term. We present the results for high contrast in permeability coefficients for two different types of distributions, see Fig. 5.1 and description in Section 5.2.6.

We have performed numerical tests using the multigrid preconditioner with overlapping Schwarz smoothers of multiplicative type. We present the performance of the multigrid preconditioners in this section for Brinkman problem with convective term. For these tests, we use problem setup as described in remark 5.2.1. We consider a constant viscosity $\nu = 0.01$ for both regions in case of Brinkman problem and $\nu = 0$ in case of Darcy problem.

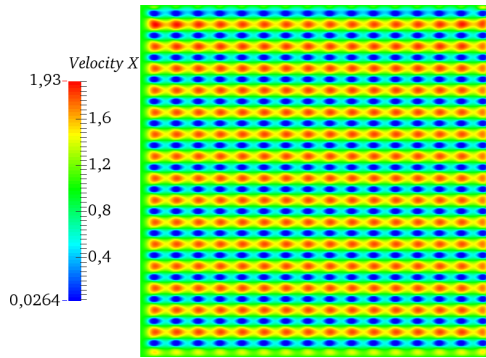
For multigrid preconditioner, we apply standard V-cycle algorithm with overlapping multiplicative Schwarz smoothers with one smoothing step at each level. We use the uniform mesh refinements and the penalty parameter in DG formulation as $\sigma_\ell = \frac{k(k+1)}{2h_\ell}$, where h_ℓ is the mesh size at level ℓ and k is the degree of polynomial. We use the finite element pair $RT_1 \times Q_1$ in all of our numerical tests. In this case, we have a nonlinear convection term. Hence, we use a Picard iteration scheme as outer solver for non-linearity and GMRES as inner solver for linear system. Picard iteration solver is set to reduce the residual to 10^{-6} . In Table 5.3, we present the iteration count of GMRES and Picard iteration for Brinkman problem with convective term using Sparse periodic geometry. In columns of Table 5.3, we show different permeability contrasts and in sub-columns, we show iterations for Picard iteration and GMRES. The rows of 5.3, represent different levels for multigrid. The coarsest level contains only one cell, so our mesh size at level 7 is $1/64$. We build

level	$\kappa = 10^4$		$\kappa = 10^5$		$\kappa = 10^6$	
	Picard	GMRES	Picard	GMRES	Picard	GMRES
7	31	4	29	4	29	4
8	31	3	27	3	26	3
9	31	3	25	3	22	3
10	26	4	19	4	14	4

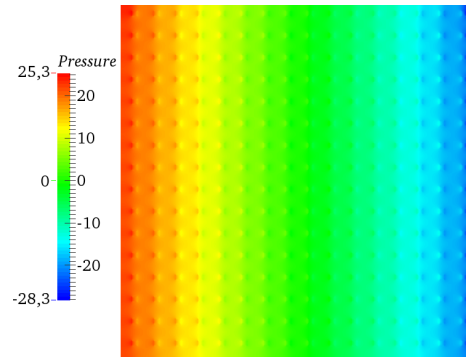
Table 5.3: Iteration count of Picard iteration and GMRES for Sparse periodic geometry

multigrid preconditioners using upscaling and downscaling as described in remark 5.2.2. We observed that our solver is robust and is independent of the mesh parameters and variations in permeability coefficients. Furthermore, we provide the numerical solution for different permeability contrast for Sparse periodic geometry in Fig. 5.7, where we show only x-component of velocity and pressure.

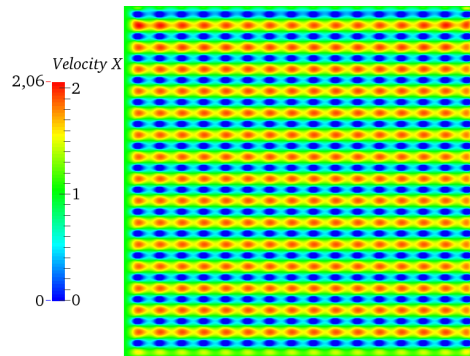
Similarly, we show the iteration count of GMRES and Picard iteration for Brinkman problem with convective term using Dense periodic geometry in Table 5.4. Where, the columns represent iterations of Picard iteration and GMRES for different permeability contrasts. The multigrid levels are presented in rows. For multigrid preconditioner, we take the same approach as for the symmetric case of Brinkman problem. We observed that our solver is independent of permeability contrast as can be seen in rows. Further, it is independent of the mesh as shown in columns. We present the numerical solution for the Brinkman solver for Dense periodic geometry in Fig. 5.8,



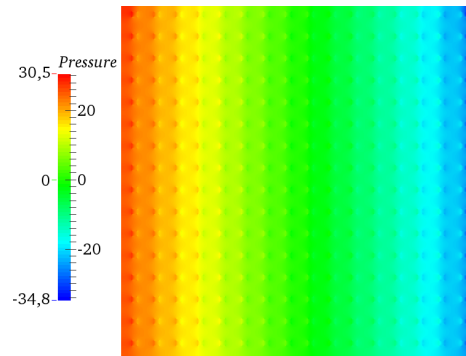
(a) Velocity x-component for $\kappa = 10^4$



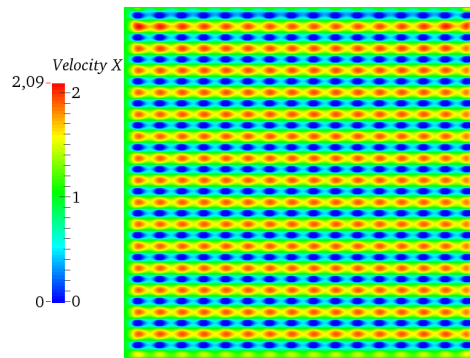
(b) Pressure for $\kappa = 10^4$



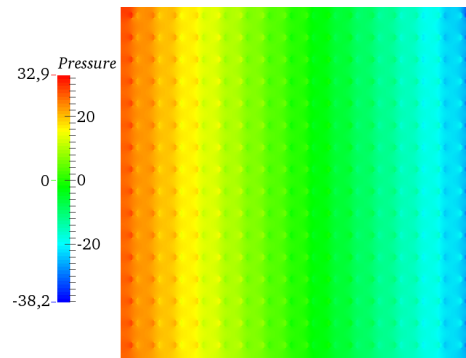
(c) Velocity x-component for $\kappa = 10^5$



(d) Pressure for $\kappa = 10^5$



(e) Velocity x-component for $\kappa = 10^6$



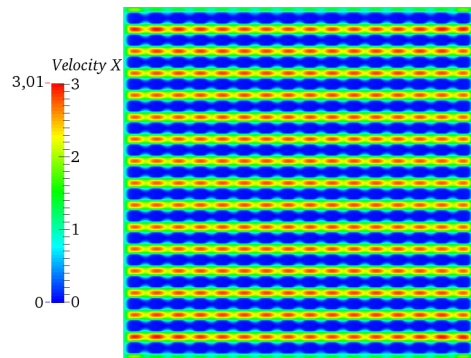
(f) Pressure for $\kappa = 10^6$

Figure 5.7: Nonlinear Brinkman: Solution in Sparse periodic geometry

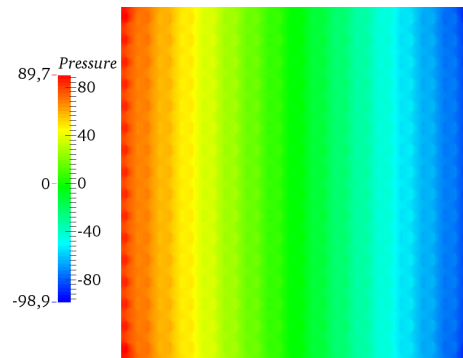
level	$\kappa = 10^4$		$\kappa = 10^5$		$\kappa = 10^6$	
	Picard	GMRES	Picard	GMRES	Picard	GMRES
7	19	3	20	4	20	4
8	22	2	24	2	25	2
9	24	2	25	2	24	3
10	22	3	21	3	17	4

Table 5.4: Iteration count of Picard iteration and GMRES for Dense periodic geometry

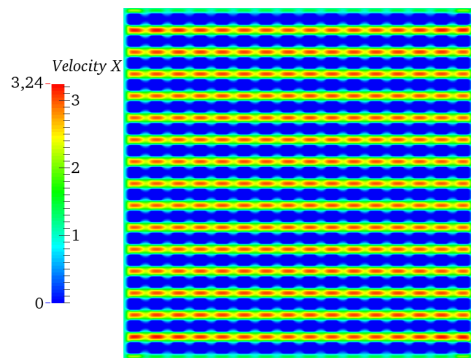
where we show only x-component of velocity and pressure for the sake of simplicity.



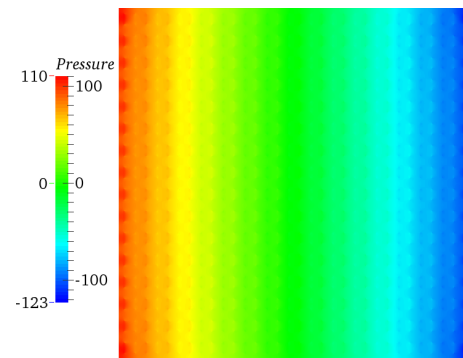
(a) Velocity x-component for $\kappa = 10^4$



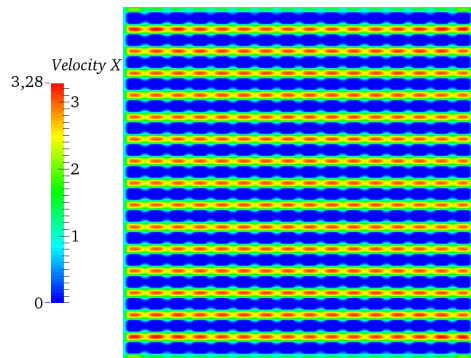
(b) Pressure for $\kappa = 10^4$



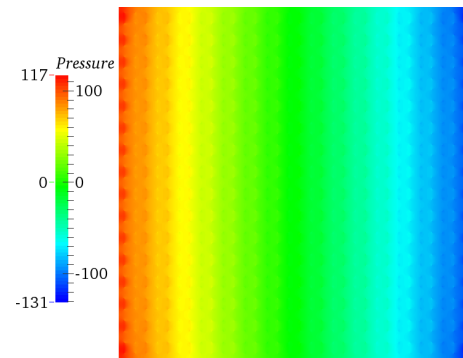
(c) Velocity x-component for $\kappa = 10^5$



(d) Pressure for $\kappa = 10^5$



(e) Velocity x-component for $\kappa = 10^6$



(f) Pressure for $\kappa = 10^6$

Figure 5.8: Nonlinear Brinkman: Solution in Dense periodic geometry

5.4 Summary

In this chapter, we have mainly presented the numerical results in two parts. First part contains the results for the Brinkman problem which have already been done by [51] and [59]. We have done the same numerical experiments for the classical test case of Dense periodic geometry and Sparse periodic geometry. We have also used a different upscaling scheme which improved the results in terms of iterations count for GMRES as compared to the aforementioned works.

The second part of the chapter contains numerical results for Brinkman model including the convective term which breaks the symmetry. By using the theory of symmetric problems and applying our solvers to non-symmetric problems, we still have reasonable agreements of numerical results with theory. The numerical results are an encouraging step in the further developments in theory.

Chapter 6

Summary

In this thesis, we have studied mainly the geometric multigrid method for the Oseen, the Navier-Stokes and the Brinkman equations. We used H^{div} -conforming finite element methods, that globally satisfy the incompressibility constraint. The multigrid preconditioners are based on overlapping Schwarz smoothers and used in combination with classical iterative solver. We have implemented the multigrid method and performed numerical experiments for flow problems.

In Chapter 3, we have mostly presented the numerical results for Oseen problem using multigrid preconditioners employing overlapping Schwarz smoothers of multiplicative type. The algebraic systems, arising from H^{div} -conforming discontinuous Galerkin discretization of Oseen equations, are non-symmetric because of the convection term. There is not enough theory of multigrid with Schwarz smoothers for non-symmetric systems. Hence, we have performed our numerical experiments aligned with the theory of symmetric problems. Our results show that multigrid preconditioners with Schwarz smoothers of

multiplicative type are robust and independent of mesh parameters for the non-symmetric systems also.

In Chapter 4, we presented extensive numerical experiment for Navier-Stokes problem. For numerical solution of Navier-Stokes equations, we first discretized the system using H^{div} -conforming discontinuous Galerkin methods. Then, we solved the resulting non-symmetric algebraic system using multigrid preconditioners with overlapping multiplicative Schwarz smoothers. In case of the Navier-Stokes problem, we have two difficulties: non-linearity and non-symmetry. For solving non-linearity we used Newton method as outer solver. We used GMRES as inner solver preconditioned with multigrid preconditioner, to solve the linear system in each Newton step. We applied the theory of symmetric problems for building our multigrid preconditioners. In view of our numerical results, we have seen the dependence of our multigrid preconditioners on mesh parameters and Reynolds number. Nonetheless, our solver is robust for cases of low Reynolds number.

In Chapter 5, we have presented the efficient solvers for Brinkman equations neglecting the convective term and then Brinkman including the convective term. Here, we also used H^{div} -conforming discontinuous Galerkin method for the discretization. Then, we applied our multigrid method to solve the resulting algebraic system. We have mainly presented the numerical results in two parts. First part contains the results for the Brinkman problem which has already been done by [51] and [59]. We have done the same numerical experiments for the classical test case of Sparse periodic geometry and Dense periodic geometry. We have used a different upscaling scheme as compared to [51, 59]. However, our upscaling scheme for multigrid preconditioner reduced

the iterations count for GMRES further. The second part of the chapter contains numerical results for the Brinkman model, including the convective term that breaks the symmetry. By using the theory of symmetric problems and applying our solvers to non-symmetric problems, we still have reasonable agreements of numerical results with theory. The numerical results are encouraging for a step forward to further developments in theory.

This work can be extended in two aspects: development of theoretical analysis for non-symmetric problems and improvement in computational methods for non-linear problems. Furthermore, we have already started computational experiment for time dependent versions of Navier-Stokes and Brinkman, which can be of great interest with respect to applications, in particular for industrial applications.

Bibliography

- [1] Robert A Adams and John JF Fournier. *Sobolev spaces*. Vol. 140. Academic press, 2003.
- [2] Grégoire Allaire. “Homogenization of the Navier-Stokes equations in open sets perforated with tiny holes I. Abstract framework, a volume distribution of holes”. In: *Archive for Rational Mechanics and Analysis* 113.3 (1991), pp. 209–259. ISSN: 1432-0673. DOI: [10.1007/BF00375065](https://doi.org/10.1007/BF00375065). URL: <http://dx.doi.org/10.1007/BF00375065>.
- [3] Todd Arbogast. “Analysis of a two-scale, locally conservative subgrid upscaling for elliptic problems”. In: *SIAM Journal on Numerical Analysis* 42.2 (2004), pp. 576–598.
- [4] Todd Arbogast and Heather L Lehr. “Homogenization of a Darcy–Stokes system modeling vuggy porous media”. In: *Computational Geosciences* 10.3 (2006), pp. 291–302.
- [5] Todd Arbogast and Hailong Xiao. “A multiscale mortar mixed space based on homogenization for heterogeneous elliptic problems”. In: *SIAM Journal on Numerical Analysis* 51.1 (2013), pp. 377–399.

- [6] Todd Arbogast et al. “A multiscale mortar mixed finite element method”. In: *Multiscale Modeling & Simulation* 6.1 (2007), pp. 319–346.
- [7] D. Arndt et al. “The deal.II Library, Version 8.5”. In: *submitted* (2017).
- [8] Douglas Arnold, Richard Falk, and Ragnar Winther. “Preconditioning in $H(\cdot)$ and applications”. In: *Mathematics of Computation of the American Mathematical Society* 66.219 (1997), pp. 957–984.
- [9] Douglas N Arnold. “An interior penalty finite element method with discontinuous elements”. In: *SIAM journal on numerical analysis* 19.4 (1982), pp. 742–760.
- [10] Douglas N Arnold, Richard S Falk, and Ragnar Winther. “Multigrid in $H(\text{div})$ and $H(\text{curl})$ ”. In: *Numerische Mathematik* 85.2 (2000), pp. 197–217.
- [11] W. Bangerth, R. Hartmann, and G. Kanschat. “deal.II – a General Purpose Object Oriented Finite Element Library”. In: *ACM Trans. Math. Softw.* 33.4 (2007), pp. 24/1–24/27.
- [12] Jürgen Bey. “Downwind Numbering: A Robust Multigrid Method for Convection”. In: *Fast Solvers for Flow Problems: Proceedings of the Tenth GAMM-Seminar Kiel, January 14–16, 1994*. Springer-Verlag, 2013, p. 63.
- [13] Giuseppe Bonfigli and Patrick Jenny. “An efficient multi-scale Poisson solver for the incompressible Navier–Stokes equations with immersed boundaries”. In: *Journal of Computational Physics* 228.12 (2009), pp. 4568–4587.

- [14] James H Bramble. *Multigrid methods*. Vol. 294. CRC Press, 1993.
- [15] James H Bramble et al. “Convergence estimates for product iterative methods with applications to domain decomposition”. In: *Mathematics of Computation* 57.195 (1991), pp. 1–21.
- [16] Franco Brezzi and Michel Fortin. *Mixed and Hybrid Finite Element Methods*. Springer-Verlag, New York, 1991.
- [17] H. C. Brinkman. “A calculation of the viscous force exerted by a flowing fluid on a dense swarm of particles”. In: *Flow, Turbulence and Combustion* 1.1 (1949), p. 27. ISSN: 1573-1987. DOI: [10.1007/BF02120313](https://doi.org/10.1007/BF02120313). URL: <http://dx.doi.org/10.1007/BF02120313>.
- [18] Erik Burman and Peter Hansbo. “A unified stabilized method for Stokes and Darcy’s equations”. In: *Journal of Computational and Applied Mathematics* 198.1 (2007), pp. 35–51.
- [19] Erik Burman and Peter Hansbo. “Stabilized Crouzeix-Raviart element for the Darcy-Stokes problem”. In: *Numerical Methods for Partial Differential Equations* 21.5 (2005), pp. 986–997.
- [20] Mingchao Cai and Mo Mu. “A multilevel decoupled method for a mixed Stokes/Darcy model”. In: *Journal of computational and applied mathematics* 236.9 (2012), pp. 2452–2465.
- [21] Bernardo Cockburn, Guido Kanschat, and Dominik Schötzau. “A locally conservative LDG method for the incompressible Navier-Stokes equations”. In: *Mathematics of Computation* 74.251 (2005), pp. 1067–1095.

- [22] Bernardo Cockburn, Guido Kanschat, and Dominik Schötzau. “A note on discontinuous Galerkin divergence-free solutions of the Navier–Stokes equations”. In: *Journal of Scientific Computing* 31.1-2 (2007), pp. 61–73.
- [23] Bernardo Cockburn, Guido Kanschat, and Dominik Schötzau. “The local discontinuous Galerkin method for the Oseen equations”. In: *Mathematics of Computation* 73.246 (2004), pp. 569–593.
- [24] Bernardo Cockburn et al. “Local discontinuous Galerkin methods for the Stokes system”. In: *SIAM Journal on Numerical Analysis* 40.1 (2002), pp. 319–343.
- [25] Carlo D’Angelo and Paolo Zunino. “A finite element method based on weighted interior penalties for heterogeneous incompressible flows”. In: *SIAM Journal on Numerical Analysis* 47.5 (2009), pp. 3990–4020.
- [26] Yalchin Efendiev, Juan Galvis, and PANAYOT S Vassilevski. “Multi-scale spectral AMGe solvers for high-contrast flow problems”. In: *ISC-Preprint, Texas A&M University* (2012).
- [27] Yalchin Efendiev, Juan Galvis, and Panayot S Vassilevski. “Spectral element agglomerate algebraic multigrid methods for elliptic problems with high-contrast coefficients”. In: *Domain decomposition methods in science and engineering XIX*. Springer, 2011, pp. 407–414.
- [28] Yalchin Efendiev and Thomas Y Hou. *Multiscale finite element methods: theory and applications*. Vol. 4. Springer Science & Business Media, 2009.

- [29] Yalchin R Efendiev, Thomas Y Hou, and Xiao-Hui Wu. “Convergence of a nonconforming multiscale finite element method”. In: *SIAM Journal on Numerical Analysis* 37.3 (2000), pp. 888–910.
- [30] Howard C Elman, David J Silvester, and Andrew J Wathen. *Finite elements and fast iterative solvers: with applications in incompressible fluid dynamics*. Oxford University Press (UK), 2014.
- [31] Howard C Elman, David J Silvester, and Andrew J Wathen. “Performance and analysis of saddle point preconditioners for the discrete steady-state Navier-Stokes equations”. In: *Numerische Mathematik* 90.4 (2002), pp. 665–688.
- [32] Richard S Falk and Michael Neilan. “Stokes complexes and the construction of stable finite elements with pointwise mass conservation”. In: *SIAM Journal on Numerical Analysis* 51.2 (2013), pp. 1308–1326.
- [33] Xiaobing Feng and Ohannes A Karakashian. “Two-level additive Schwarz methods for a discontinuous Galerkin approximation of second order elliptic problems”. In: *SIAM Journal on Numerical Analysis* 39.4 (2001), pp. 1343–1365.
- [34] Vivette Girault and Pierre-Arnaud Raviart. *Finite element methods for Navier-Stokes equations: theory and algorithms*. Vol. 5. Springer Science & Business Media, 2012.
- [35] Kanschat Guido. “Block preconditioners for LDG discretizations of linear incompressible flow problems”. In: *Journal of Scientific Computing* 22.1 (2005), pp. 371–384.

- [36] Johnny Guzmán and Michael Neilan. “Conforming and divergence-free Stokes elements on general triangular meshes”. In: *Mathematics of Computation* 83.285 (2014), pp. 15–36.
- [37] Wolfgang Hackbusch and Thomas Probst. “Downwind Gauss-Seidel smoothing for convection dominated problems”. In: *Numerical linear algebra with applications* 4.2 (1997), pp. 85–102.
- [38] Hadi Hajibeygi et al. “Iterative multiscale finite-volume method”. In: *Journal of Computational Physics* 227.19 (2008), pp. 8604–8621.
- [39] Antti Hannukainen, Mika Juntunen, and Rolf Stenberg. “Computations with finite element methods for the Brinkman problem”. In: *Computational Geosciences* 15.1 (2011), pp. 155–166.
- [40] Peter Hansbo and Mika Juntunen. “Weakly imposed Dirichlet boundary conditions for the Brinkman model of porous media flow”. In: *Applied Numerical Mathematics* 59.6 (2009), pp. 1274–1289.
- [41] Peter Hansbo and Mats G Larson. “Discontinuous Galerkin methods for incompressible and nearly incompressible elasticity by Nitsche’s method”. In: *Computer methods in applied mechanics and engineering* 191.17 (2002), pp. 1895–1908.
- [42] Ralf Hiptmair. “Multigrid method for Maxwell’s equations”. In: *SIAM Journal on Numerical Analysis* 36.1 (1998), pp. 204–225.
- [43] Ralf Hiptmair and Jinchao Xu. “Preface: Special issue on adaptive and multilevel methods in computational electromagnetics”. In: *Journal of Computational Mathematics* 27 (2009), pp. 561–562.

- [44] O. Iliev, R. Lazarov, and J. Willems. “Variational Multiscale Finite Element Method for Flows in Highly Porous Media”. In: *Multiscale Modeling & Simulation* 2011.9 (2011 Oct). ISSN: 1540-3459. DOI: [10.1137/10079940X](https://doi.org/10.1137/10079940X). URL: <http://hdl.handle.net/10754/600164>.
- [45] Oleg Iliev, Raytcho Lazarov, and Joerg Willems. “Fast numerical up-scaling of heat equation for fibrous materials”. In: *Computing and Visualization in Science* 13.6 (2010), pp. 275–285.
- [46] Oleg P. Iliev, Raytcho D. Lazarov, and Joerg Willems. “Discontinuous Galerkin Subgrid Finite Element Method for Heterogeneous Brinkman’s Equations”. In: *Large-Scale Scientific Computing: 7th International Conference, LSSC 2009, Sozopol, Bulgaria, June 4-8, 2009. Revised Papers*. Ed. by Ivan Lirkov, Svetozar Margenov, and Jerzy Waśniewski. Berlin, Heidelberg: Springer Berlin Heidelberg, 2010, pp. 14–25. ISBN: 978-3-642-12535-5. DOI: [10.1007/978-3-642-12535-5_2](https://doi.org/10.1007/978-3-642-12535-5_2). URL: http://dx.doi.org/10.1007/978-3-642-12535-5_2.
- [47] Patrick Jenny and Ivan Lunati. “Multi-Scale Finite-Volume Method for Elliptic Problems with Heterogeneous Coefficients and Source Terms”. In: *PAMM* 6.1 (2006), pp. 485–486.
- [48] Guido Kanschat. “Divergence-free discontinuous Galerkin schemes for the Stokes equations and the MAC scheme”. In: *International journal for numerical methods in fluids* 56.7 (2008), pp. 941–950.
- [49] Guido Kanschat. “Preconditioning methods for local discontinuous Galerkin discretizations”. In: *SIAM Journal on Scientific Computing* 25.3 (2003), pp. 815–831.

- [50] Guido Kanschat. “Robust smoothers for high-order discontinuous Galerkin discretizations of advection–diffusion problems”. In: *Journal of Computational and Applied Mathematics* 218.1 (2008), pp. 53–60.
- [51] Guido Kanschat, Raytcho Lazarov, and Youli Mao. “Geometric Multigrid for Darcy and Brinkman models of flows in highly heterogeneous porous media: A numerical study”. In: *Journal of Computational and Applied Mathematics* (2016).
- [52] Guido Kanschat and Youli Mao. “Multigrid methods for Hdiv-conforming discontinuous Galerkin methods for the Stokes equations”. In: *Journal of Numerical Mathematics* 23.1 (2015), pp. 51–66.
- [53] Guido Kanschat and Béatrice Riviere. “A strongly conservative finite element method for the coupling of Stokes and Darcy flow”. In: *Journal of Computational Physics* 229.17 (2010), pp. 5933–5943.
- [54] Guido Kanschat and Dominik Schötzau. “Energy norm a posteriori error estimation for divergence-free discontinuous Galerkin approximations of the Navier–Stokes equations”. In: *International Journal for Numerical Methods in Fluids* 57.9 (2008), pp. 1093–1113.
- [55] David Kay, Daniel Loghin, and Andrew Wathen. “A Preconditioner for the Steady-State Navier–Stokes Equations”. In: *SIAM Journal on Scientific Computing* 24.1 (2002), pp. 237–256.
- [56] Juho Könnö and Rolf Stenberg. “H (div)-conforming finite elements for the Brinkman problem”. In: *Mathematical Models and Methods in Applied Sciences* 21.11 (2011), pp. 2227–2248.

- [57] L. I. G. Kovasznay. “Laminar flow behind a two-dimensional grid”. In: *Mathematical Proceedings of the Cambridge Philosophical Society* 44.1 (Jan. 1948), pp. 58–62.
- [58] William J Layton, Friedhelm Schieweck, and Ivan Yotov. “Coupling fluid flow with porous media flow”. In: *SIAM Journal on Numerical Analysis* 40.6 (2002), pp. 2195–2218.
- [59] Youli Mao. “Geometric Multigrid Methods for Flow Problems in Highly Heterogeneous Porous Media”. PhD thesis. 2014.
- [60] Kent Andre Mardal, Xue-Cheng Tai, and Ragnar Winther. “A robust finite element method for Darcy–Stokes flow”. In: *SIAM Journal on Numerical Analysis* 40.5 (2002), pp. 1605–1631.
- [61] Mo Mu and Jinchao Xu. “A two-grid method of a mixed Stokes–Darcy model for coupling fluid flow with porous media flow”. In: *SIAM journal on numerical analysis* 45.5 (2007), pp. 1801–1813.
- [62] Malcolm F Murphy, Gene H Golub, and Andrew J Wathen. “A note on preconditioning for indefinite linear systems”. In: *SIAM Journal on Scientific Computing* 21.6 (2000), pp. 1969–1972.
- [63] Joachim Nitsche. “Über ein Variationsprinzip zur Lösung von Dirichlet-Problemem bei Verwendung von Teilräumen, die keinen Randbedingungen unterworfen sind”. In: *Abhandlungen aus dem mathematischen Seminar der Universität Hamburg*. Vol. 36. 1. Springer. 1971, pp. 9–15.
- [64] Alfio Quarteroni and Alberto Valli. *Numerical approximation of partial differential equations*. Vol. 23. Springer Science & Business Media, 2008.

- [65] Pierre-Arnaud Raviart and Jean-Marie Thomas. “A mixed finite element method for 2-nd order elliptic problems”. In: *Mathematical aspects of finite element methods*. Springer, 1977, pp. 292–315.
- [66] Youcef Saad and Martin H Schultz. “GMRES: A generalized minimal residual algorithm for solving nonsymmetric linear systems”. In: *SIAM Journal on scientific and statistical computing* 7.3 (1986), pp. 856–869.
- [67] Joachim Schöberl. “Multigrid methods for a parameter dependent problem in primal variables”. In: *Numerische Mathematik* 84.1 (1999), pp. 97–119.
- [68] Joachim Schöberl. “Robust multigrid methods for parameter dependent problems”. PhD thesis. Johannes Kepler Universität Linz, 1999.
- [69] Dominik Schötzau, Christoph Schwab, and Andrea Toselli. “Mixed hp-DGFEM for incompressible flows”. In: *SIAM Journal on Numerical Analysis* 40.6 (2002), pp. 2171–2194.
- [70] LR Scott and Michael Vogelius. “Norm estimates for a maximal right inverse of the divergence operator in spaces of piecewise polynomials”. In: *RAIRO-Modélisation mathématique et analyse numérique* 19.1 (1985), pp. 111–143.
- [71] Andrea Toselli and Olof B Widlund. *Domain decomposition methods: algorithms and theory*. Vol. 34. Springer, 2005.
- [72] S Pratap Vanka. “Block-implicit multigrid solution of Navier-Stokes equations in primitive variables”. In: *Journal of Computational Physics* 65.1 (1986), pp. 138–158.

- [73] Panayot S Vassilevski and Umberto Villa. “A block-diagonal algebraic multigrid preconditioner for the Brinkman problem”. In: *SIAM Journal on Scientific Computing* 35.5 (2013), S3–S17.
- [74] Panayot S Vassilevski and Umberto Villa. “A mixed formulation for the Brinkman problem”. In: *SIAM Journal on Numerical Analysis* 52.1 (2014), pp. 258–281.
- [75] Michael Vogelius. “A right-inverse for the divergence operator in spaces of piecewise polynomials”. In: *Numerische Mathematik* 41.1 (1983), pp. 19–37.
- [76] Junping Wang and Xiu Ye. “New finite element methods in computational fluid dynamics by H (div) elements”. In: *SIAM Journal on Numerical Analysis* 45.3 (2007), pp. 1269–1286.
- [77] Jörg Willems. “Numerical upscaling for multiscale flow problems”. PhD thesis. Technische Universität Kaiserslautern Fachbereich Mathematik, 2009.
- [78] Xiaoping Xie, Jinchao Xu, and Guangri Xue. “Uniformly-stable finite element methods for Darcy-Stokes-Brinkman models”. In: *Journal of Computational Mathematics* (2008), pp. 437–455.
- [79] Jinchao Xu. “Iterative methods by space decomposition and subspace correction”. In: *SIAM review* 34.4 (1992), pp. 581–613.
- [80] Xuejun Xu and Shangyou Zhang. “A new divergence-free interpolation operator with applications to the Darcy–Stokes–Brinkman equations”. In: *SIAM Journal on Scientific Computing* 32.2 (2010), pp. 855–874.

- [81] Shangyou Zhang. “A family of 3D continuously differentiable finite elements on tetrahedral grids”. In: *Applied Numerical Mathematics* 59.1 (2009), pp. 219–233.
- [82] Shangyou Zhang. “A Family of $Q_{k+1,k,k+1}$ Divergence-Free Finite Elements on Rectangular Grids”. In: *SIAM Journal on Numerical Analysis* 47.3 (2009), pp. 2090–2107.